An updated sulfate transporter phylogeny uncovers a perennial-specific subgroup associated with lignification

Samantha M. Surber[1,2], Chen Hsieh[3], Lan Na[4], Scott A. Harding[5], Chung-Jui Tsai[1,2,3,5,6]

[1] Department of Plant Biology, University of Georgia, Athens, GA 30602, USA
[2] Center for Bioenergy Innovation, Oak Ridge National Laboratory, Oak Ridge, TN 37831, USA
[3] Institute of Bioinformatics, University of Georgia, Athens, GA 30602, USA
[4] Complex Carbohydrate Research Center, University of Georgia, Athens, GA 30602, USA
[5] Warnell School of Forestry, University of Georgia, Athens, GA 30602, USA
[6] Department of Genetics, University of Georgia, Athens, GA 30602, USA

Running title: SULTR phylogeny and lignin-specific PtaSULTR3.2

Keywords: SULTR, Populus, sulfur assimilation, lignin biosynthesis, xylem

Corresponding author: Chung-Jui Tsai (cjtsai@uga.edu), 120 E. Green Street, Athens, GA 30602, USA

ABSTRACT

Sulfate-proton co-transporters (SULTRs) mediate sulfate uptake, transport, storage, and assimilation in plants. The SULTR family has historically been classified into four groups (SULTR1-SULTR4), with well-characterized roles for SULTR groups 1, 2, and 4. However, the functions of the large and diverse SULTR3 group remain poorly understood. Here, we present an updated phylogenetic analysis of SULTRs across angiosperms, including multiple early-divergent lineages. Our results suggest that the enigmatic SULTR3 group comprises four distinct subfamilies that predate the emergence of angiosperms, providing a basis for reclassifying the SULTR family into seven subfamilies. This expanded classification is supported by subfamily-specific gene structures and amino acid substitutions in the substrate-binding pocket. Structural modeling identified three serine residues uniquely lining the substrate-binding pocket of SULTR3.4, enabling three hydrogen bonds with the phosphate ion. The data support the proposed neofunctionalization of this subfamily for phosphate allocation within vascular tissues. Transcriptome analysis of *Populus tremula* × *alba* revealed divergent tissue expression preferences among *SULTR* subfamilies and between genome duplicates. We observed partitioned expression in vascular tissues among the four *SULTR3* subfamilies, with *PtaSULTR3.4a* and *PtaSULTR3.2a* preferentially expressed in primary and secondary xylem, respectively. Gene coexpression analysis revealed coordinated expression of *PtaSULTR3.4a* with genes involved in phosphate starvation responses and nutrient transport, consistent with a potential role in phosphate homeostasis. In contrast, *PtaSULTR3.2a* was strongly coexpressed with lignification and one-carbon metabolism genes and their upstream transcription regulators. *PtaSULTR3.2a* belongs to a eudicot-specific branch of the SULTR3.1 subfamily found only in perennial species, suggesting a specialized role in lignifying tissues. Together, our findings provide a refined phylogenetic framework for the SULTR family and suggest that the expanded SULTR3 subfamilies have undergone neofunctionalization during the evolution of vascular and perennial plants.

63 **INTRODUCTION**

64

65 Sulfur is an essential plant macronutrient taken up from the soil as inorganic sulfate (Kopriva et al. 2019).
66 Uptake and plantwide distribution are mediated by a family of sulfate-proton co-transporters (SULTRs)
67 historically classified into four groups, referred to as SULTR1 to SULTR4 (Takahashi et al. 2000). This
68 Arabidopsis (*Arabidopsis thaliana*)-based nomenclature has been followed in many subsequent
69 phylogenetic analyses (Takahashi et al. 2012; Gallardo et al. 2014; Ding et al. 2016; Xun et al. 2021; Zhao
70 et al. 2022; Chen et al. 2024). Two recent studies classified the SULTR family into five groups but with
71 inconsistent nomenclature and memberships (Heidari et al. 2023; Puresmaeli et al. 2023). Meanwhile,
72 molecular characterization continues to shed light on all SULTR groups as evidenced by their varied
73 subcellular localization, transport kinetics, tissue expression, and stress responsiveness (Takahashi 2019).

74

75 Among the different groups, SULTR4 transporters are tonoplast-localized and facilitate sulfate efflux from
76 the vacuole (Kataoka et al. 2004b). SULTR1 and SULTR2 members are plasma membrane-localized with
77 SULTR1 being high-affinity transporters involved in sulfate uptake by the roots (Takahashi et al. 2000;
78 Yoshimoto et al. 2002), and SULTR2 being low-affinity transporters expressed primarily in the root
79 cylinder for root-to-shoot sulfate transport (Takahashi et al. 1997; Takahashi et al. 2000). SULTR3 is the
80 largest and most diverse group, with five genes in Arabidopsis—*AtSULTR3.1*, *AtSULTR3.2*, *AtSULTR3.3*,
81 *AtSULTR3.4,* and *AtSULTR3.5* (Zuber et al. 2010; Takahashi et al. 2012). The subcellular distribution and
82 function of SULTR3 members are less precisely known but recent reports suggest localization to the
83 plasma membrane (Kataoka et al. 2004a; Yamaji et al. 2017; Ding et al. 2020), endoplasmic reticulum
84 (Zhao et al. 2016), and/or chloroplast (Cao et al. 2013; Chen et al. 2019).

85

86 SULTR3 members are enigmatic with respect to their sulfate transport capabilities. AtSULTR3.1,
87 AtSULTR3.2, and AtSULTR3.3 did not show sulfate uptake activity in yeast (Takahashi et al. 2000). To date,
88 successful restoration of yeast mutant growth on sulfate-containing media by SULTR3 has only been
89 reported for LjSST1 (SULTR3.5) of lotus (*Lotus japonicus*) and MhSULTR3.1a of apple (*Malus hupehensis*),
90 although the uptake kinetics were not determined (Krusell et al. 2005; Xun et al. 2021). Cao et al. (2013)
91 used individual *sultr3* mutants to show that all Arabidopsis SULTR3 members, except AtSULTR3.5,
92 contribute substantially to sulfate uptake by isolated chloroplasts. Although AtSULTR3.5 alone does not
93 support sulfate uptake by isolated Arabidopsis chloroplasts or in yeast, its co-expression with *AtSULTR2.1*
94 improved growth of yeast mutants over those expressing *AtSULTR2.1* alone (Kataoka et al. 2004a). This

95 cooperation of AtSULTR3.5 and AtSULTR2.1 in the vasculature contributes to root-to-shoot sulfate
96 transport in Arabidopsis (Kataoka et al. 2004a). In rice (*Oryza sativa*), two independent *low phytic acid*
97 (*lpa*) mutant alleles were both mapped to *OsSULTR3.3*, even though no *in vitro* transport activity of
98 OsSULTR3.3 for sulfate, phosphate, inositol, or inositol triphosphate could be demonstrated in yeasts or
99 *Xenopus* oocytes (Zhao et al. 2016). Similarly, SULTR3.4 was independently characterized as a SULTR-like
100 phosphorus distribution transporter (SPDT) involved in phosphate allocation from xylem to developing
101 tissues in rice, barley (*Hordeum vulgare*), and Arabidopsis (Yamaji et al. 2017; Ding et al. 2020; Gu et al.
102 2022). OsSULTR3.4, HvSULTR3.4, and AtSULTR3.4 all function as an influx transporter for phosphate, but
103 not sulfate, in oocytes, and their knockout mutants showed impaired phosphorus distribution to
104 developing organs (Yamaji et al. 2017; Ding et al. 2020; Gu et al. 2022). These studies highlight some of
105 the ongoing challenges in elucidating the evolution and function of the diverse SULTR3 group.
106
107 *SULTR* gene expression is sensitive to abiotic stressors, including drought and salt, in Arabidopsis (Cao et
108 al. 2014), barrelclover (*Medicago truncatula*) (Gallardo et al. 2014), poplar (*Populus trichocarpa*)
109 (Malcheska et al. 2017), maize (*Zea mays*) (Huang et al. 2018), wheat (*Triticum turgidum* L. ssp.
110 *durum*)(Puresmaeli et al. 2023), and soybean (*Glycine max*) (Zhou et al. 2024). The responsiveness of
111 *SULTR* genes to drought and other abiotic stresses varies between studies in part because expression is
112 modulated not only by plant sulfur status (Vidmar et al. 1999; Takahashi et al. 2000; Rouached et al.
113 2008; Maruyama-Nakashita et al. 2015), but also by stress hormones like ABA (abscisic acid) and MeJA
114 (methyl jasmonic acid) (Cao et al. 2014; Xun et al. 2021). Notably, four of five *AtSULTR3* genes were
115 identified among the 124 transporter transcripts enriched in guard cells (Bauer et al. 2013). Moreover,
116 quintuple *sultr3* mutants showed impaired sulfate uptake for stress-induced ABA synthesis in Arabidopsis
117 (Chen et al. 2019). This supports sulfate as a xylem-borne signal that precedes localized ABA biosynthesis
118 and stomatal closure in response to drought (Ernst et al. 2010; Malcheska et al. 2017; Batool et al. 2018).
119
120 Studies on gene expression and the seasonal dynamics of wood and xylem sap sulfate abundance in
121 *Populus tremula* × *alba* have provided additional insights into the function of SULTR3 in stems. The
122 transcripts of *PtaSULTR3.1b*, *PtaSULTR3.2a*, and *PtaSULTR3.3a* peaked during active growth in the
123 summer (Dürr et al. 2010; Ko et al. 2011; Malcheska et al. 2013). The hydraulic transport network for
124 long-distance and lateral movements of solutes and water are more complex in large stature trees
125 (Pfautsch et al. 2015). In addition, the formation of large woody sinks depends heavily on sulfur
126 assimilation to supply one-carbon (C1) units for methyl-intensive lignification (Rajinikanth et al. 2007).

127 Here, we report an updated SULTR phylogeny using 20 angiosperm species, including several woody
128 perennials where SULTR function has been little explored. The inclusion of basal lineages revealed a
129 much more ancient origin of the expanded SULTR3 group than previously recognized. Multiple lines of
130 evidence, including gene structure, protein structural modeling with differential substrate docking, and
131 gene expression, support the functional divergence of SULTR3. We also discuss the potential association
132 of certain SULTR3 members with lignification in *Populus*.
133
134

135 **METHODS**

136

137 *Sequence collection and annotation*
138 SULTR protein sequences from 22 species were obtained from Phytozome v13 (https://phytozome-
139 next.jgi.doe.gov/)(Goodstein et al. 2012), and the list, including gene models, genome version, and
140 species, is provided in Supplemental Table S1. Sequences were aligned using the multiple sequence
141 alignment tool, T-Coffee (Notredame et al. 2000) for inspection. Sequences with large gaps,
142 misalignment, and/or gene structure misannotation were manually curated, sometimes in consultation
143 with independently annotated genome versions at NCBI. The full sequence dataset has been deposited
144 with the U.S. Department of Energy's Office of Scientific and Technical Information (OSTI.gov). Exon-
145 intron annotation was retrieved from Phytozome for spikemoss (*Selaginella moellendorffii*), moss
146 (*Physcomitrium patens*), pineapple (*Ananas comosus*), blue columbine (*Aquilegia coerulea*), Arabidopsis
147 (*Arabidopsis thaliana*), poplar (*Populus trichocarpa*), rice (*Oryza sativa*), and sorghum (*Sorghum bicolor*)
148 and the structure was illustrated using Gene Structure Draw Tool (https://www.bioinformatics.uni-
149 muenster.de/tools/strdraw/).
150

151 *Phylogenetic reconstruction*
152 Preliminary alignment of all 262 protein sequences performed with T-Coffee on EMBL-EBI (Madeira et al.
153 2024) was used in a model test with ModelFinder (Kalyaanamoorthy et al. 2017) implemented in IQ-
154 TREE v1.6.12 (Nguyen et al. 2015). This revealed a general JTT model for amino acid substitution rate
155 (Jones et al. 1992), gamma rate of 4 (G4), allowing for a proportion of invariable sites (I), and empirical
156 frequencies (F) [JTT+G4+I+F]. The model JTT+G4+I+F was used for maximum likelihood inference for
157 phylogenetic tree construction with IQ-TREE v1.6.12 and 1000 ultrafast bootstrap cycles. Trees were

158 visualized on TreeViewer (https://treeviewer.org/) (Bianchini and Sánchez-Baracaldo 2024) and edited in
159 MEGA-X (Kumar et al. 2018) for presentation. The full tree (Figure 1) is unrooted, while the SULTR3-
160 specific tree (Figure 2) is rooted on the basal spikemoss SULTR3 sequences.
161
162 *Substrate binding site alignment and protein structural modeling*
163 All poplar and Arabidopsis SULTR protein sequences were aligned as above. The structure-resolved
164 AtSULTR4.1 (AT5G13550) protein sequence was used as the reference to annotate key residues involved
165 in substrate and co-substrate binding and interactions according to Wang et al. (2021). Protein
166 sequences for PtaSULTR3.1a, PtaSULTR3.2a, PtaSULTR3.3a, PtaSULTR3.4a, and PtaSULTR3.5 from *Populus*
167 *tremula* × *alba* INRA 717-1B4 were used for AlphaFold3 (Abramson et al. 2024) modeling to investigate
168 substrate-binding pocket architecture and potential determinants of substrate specificity. AlphaFold3
169 models were generated using default parameters (seed 1), without template constraints. Each model
170 was visually inspected for fold quality and overall membrane topology. Structural comparisons and
171 visualizations were performed using PyMOL v3.0.0 (The PyMOL Molecular Graphics System, Schrödinger,
172 LLC).
173
174 *Gene expression analysis*
175 RNA-Seq datasets from published *Populus tremula* × *alba* studies (Swamy et al. 2015; Xue et al. 2016;
176 Tsai et al. 2020; Zhou et al. 2023) were obtained from the NCBI Short Read Archive (SRA) using the
177 `nfcore/fetchngs` pipeline (v1.11.0) (Ewels et al. 2020). Quality control and read trimming were
178 performed using Cutadapt v4.4 (Martin 2011) with parameters -q 30, -m 30, and --trim-n. Reads were
179 mapped to the *P. tremula* subgenome (*Populus tremula* × *alba* HAP1 v5.1) of the hybrid (Zhou et al.
180 2023) available on Phytozome v13. For expression quantification, kallisto v0.48.0 (Bray et al. 2016) was
181 used, with a *k*-mer size of 21 for indexing. Single-end reads were quantified with an estimated average
182 fragment length of 200 and a standard deviation of 20. Paired-end reads were quantified without the
183 stranded option. *SULTR* gene expression values were extracted and statistical significance of treatment
184 responses was performed using PRISM v10.1.0 (GraphPad Software, Boston, MA). Heatmap and bar
185 graphs were generated using Excel.
186
187 Gene coexpression analysis was performed using 174 RNA-seq datasets from *Populus tremula* × *alba*
188 stem vascular tissues, excluding the four studies cited above (Swamy et al. 2015; Xue et al. 2016; Tsai et
189 al. 2020; Zhou et al. 2023). The full list of datasets is provided in Supplemental Table S2. Data were

190 similarly processed to obtain expression values. Genes with low expression (TPM < 5 in all samples) were
191 filtered out and only those with a coefficient of variance (CV) > 50% were retained. Pairwise Pearson
192 correlation coefficients (PCC) were calculated between each of the remaining 19,787 genes and either
193 *PtaSULTR3.2a* or *PtaSULTR3.4a* across the 174 samples (Supplemental Table S3) using a python script
194 available at https://github.com/TsailabBioinformatics/sultr-coexpression-utils. Genes with PCC $\geq$ 0.7
195 relative to *PtaSULTR3.2a* or *PtaSULTR3.4a* were extracted for Gene Ontology (GO) enrichment using
196 ShinyGO v0.77 (Ge et al. 2020) implemented at http://aspendb.uga.edu/ShinyGO/. Further examination
197 of *SULTR3.2a* and *SULTR3.4a* expression in response to transgenic perturbations of the lignin
198 biosynthetic pathway in *P. trichocarpa* was based on the study by Wang et al. (2018). The list of datasets
199 is provided in Supplemental Table S4.
200
201
202 **RESULTS**
203
204 **Differential expansion of SULTR subfamilies**
205 A total of 262 SULTR protein sequences from 20 angiosperms and two early-divergent land plant lineages
206 were retrieved from Phytozome v13 (Goodstein et al. 2012) (https://phytozome-next.jgi.doe.gov/) (Table
207 1). These SULTR proteins are typically annotated based on their Arabidopsis orthologs into four groups,
208 SULTR1 to SULTR4 (Takahashi et al. 2000; Takahashi et al. 2012). The number of sequences per group
209 varies due to differential gene expansion among the species studied. The SULTR4 subfamily consists of
210 one or two sequences in each sampled taxon, while the other three groups show varied expansions.
211 SULTR3 has the highest number of sequences, followed by SULTR1, whereas SULTR2 exhibits a modest
212 expansion, observed only in some eudicot species (Table 1).
213
214 We constructed a SULTR phylogenetic tree using maximum likelihood inference with IQ-TREE (Nguyen et
215 al. 2015) (Figure 1). The SULTR members formed distinct clusters in a topology consistent with previous
216 reports (Takahashi et al. 2012; Ding et al. 2016; Zhao et al. 2022; Chen et al. 2024). This topology
217 suggests the existence of two ancient clades, based on the placement of SULTRs from the bryophyte
218 moss (*Physcomitrella patens*), as also suggested by Takahashi et al. (2012). The smaller Ancient Clade I
219 (AC-I) comprises the tonoplast SULTR4, whereas the larger Ancient Clade II (AC-II) encompasses the
220 other three SULTR groups (Figure 1). Within AC-II, the ancient vascular plant spikemoss (*Selaginella*

221 *moellendorffii*) contains two distinct groups that are basal to two subclades: one represented by SULTR1-
222 SULTR2 (referred to as AC-IIA) and the other by SULTR3 (AC-IIB). This suggests that the divergence of the
223 two subclades coincides with the evolution of vascular plants (Figure 1).
224
225 **SULTR1 and SULTR2 originate from ancient local duplication**
226 AC-IIA consists of two strongly supported nodes represented by the SULTR1 and SULTR2 subfamilies.
227 Both subfamilies are evolutionarily conserved in angiosperms, including the basal lineages Amborella
228 (*Amborella trichopoda*) and tulip tree (*Liriodendron tulipifera*). Interestingly, in both genomes, *SULTR1*
229 and *SULTR2* are found in close proximity with a divergent (head-to-head) orientation. This head-to-head
230 pattern has been maintained in nearly all sampled angiosperm taxa, despite lineage-specific variations,
231 including additional whole-genome or tandem duplications (see below, Supplemental Table S1). This
232 suggests that *SULTR1* and *SULTR2* originated from a local duplication event before the advent of
233 angiosperms. The data further indicates that the proximally located and oppositely oriented *SULTR1* and
234 *SULTR2* copies are likely the founding members of each subfamily.
235
236 Monocot SULTR1s formed two clusters, each represented by all sampled taxa, including the basal lineage
237 *Ananas comosus* (pineapple) (Figure 1). This suggests their divergence early during monocot evolution.
238 Eudicot SULTR1s also formed two distinct clusters. The smaller cluster has limited species representation,
239 and there is only a single SULTR1 in the basal eudicot blue columbine (*Aquilegia coerulea*)(Figure 1). This
240 suggests that the expansion of SULTR1 in eudicots occurred later and only in certain taxa. In the smaller
241 eudicot SULTR1 cluster, four of the eight species—eucalyptus (*Eucalyptus grandis*), lettuce (*Lactuca*
242 *sativa*), monkey flower (*Mimulus guttatus*), and oak (*Quercus rubra*)—harbor tandem duplicates
243 (Supplemental Table S1). This suggests a tendency for lineage-specific local amplification of this SULTR1
244 subgroup.
245
246 The SULTR2 subfamily is smaller than SULTR1, with 1-2 copies of the two basal angiosperm lineages and
247 monocots (Figure 1, Table 1). However, the SULTR2 subfamily size is more variable among eudicots,
248 ranging from a complete absence in blue columbine to four to eight copies in the legumes (Table 1). In
249 the latter case, we detected whole genome, tandem, and other duplication events both before and after
250 the split of barrelclover and soybean, leading to a disproportionately expanded SULTR2 subfamily in
251 these lineages (Supplemental Table S1).
252

253 **SULTR3 encompasses distinct subfamilies predating angiosperm evolution**

254 AC-IIB encompasses the entire SULTR3 group, with spikemoss members at the basal position (Figure 1).
255 This supports the vascular-specific origin of SULTR3s as previously suggested (Takahashi et al. 2012). Like
256 AC-IIA, AC-IIB is divided into two well-supported nodes, each containing two distinct branches. The first
257 node, hereafter AC-IIB-1, includes the SULTR3.1/3.2 and SULTR3.5 branches, while the second node, AC-
258 IIB-2, comprises the SULTR3.3 and SULTR3.4 branches (Figure 1). Each of these four branches contains
259 one or two members from Amborella and tulip tree, which are sister to all flowering plants (Table 1). This
260 indicates that, like SULTR1 and SULTR2, the four SULTR3 branches evolved before the emergence of
261 angiosperms.

262

263 To better understand the evolutionary history of AC-IIB, we constructed a phylogenetic tree using only
264 SULTR3 sequences (Figure 2). The overall topology mirrors that of the AC-IIB group in Figure 1, with
265 angiosperm members clustering into four branches predating the emergence of Amborella and tulip
266 tree. Three of the four branches correspond to the SULTR3.3, SULTR3.4, and SULTR3.5 subfamilies, each
267 with distinct monocot and dicot groups consistent with their early divergence during angiosperm
268 evolution (Figure 2). Most species are represented by a single copy, while others harbor two to four
269 paralogs (Table 1).

270

271 The SULTR3.1 branch (also called SULTR3.1/3.2 branch in previous papers, see below) has substantially
272 expanded in both monocots and eudicots after their split. Within the monocots, we identified two
273 strongly supported subgroups for grass SULTR3.1s, rooted with the lone member of pineapple (Figure 2),
274 indicating their origin from a grass-specific duplication event (Figure 2). We also observed two distinct
275 subgroups for eudicots, including blue columbine, indicating their divergence predates the common
276 ancestor of eudicots (Figure 2). The larger subgroup includes all 12 sampled eudicot taxa, many of which
277 have additional paralogs due to lineage-specific duplications. Examples include Brassicaceae (Arabidopsis
278 AtSULTR3.1 and AtSULTR3.2), Salicoid (poplar PtSULTR3.1a and PtSULTR3.1b), and legume-specific
279 duplications (Figure 2). In contrast, the smaller eudicot subgroup is only retained in blue columbine and
280 six other sampled taxa in both rosids and asterids, all of which are perennial species (Figure 2). Distinct
281 orthologs were also identified in other perennial eudicot genomes available on Phytozome v13, such as
282 birch (*Betula platyphylla*), papaya (*Carica papaya*), chestnut (*Castanea dentata*), orange (*Citrus sinensis*),
283 cassava (*Manihot esculenta*), peach (*Prunus persica*), and castor bean (*Ricinus communis*) of rosid, and

284 coffee (*Coffea arabica*) and hydrangea (*Hydrangea quercifolia*) of asterids. These findings suggest that
285 this SULTR3.1 subgroup may play an important role in the functionality of perennial species.
286
287 The duplication history of the SULTR3.1 branch has led to inconsistent gene and subfamily
288 nomenclatures in the literature. Specifically, Arabidopsis AtSULTR3.1 and AtSULTR3.2 are paralogs within
289 the same SULTR3.1 (large) subgroup, unlike AtSULTR3.3, AtSULTR3.4, and AtSULTR3.5 which represent
290 phylogenetically distinct subfamilies. In poplar, PtSULTR3.1 and PtSULTR3.2 are descendants of the
291 ancestral eudicot duplication in the larger and smaller SULTR3.1 subgroups, respectively, with their
292 Salicoid paralogs designated with "a" and "b" suffixes (*e.g.*, PtSULTR3.1a and PtSULTR3.1b) in the
293 literature (Dürr et al. 2010; Malcheska et al. 2017). In these examples, AtSULTR3.1/3.2 are orthologous to
294 PtSULTR3.1a/b, while the perennial-specific PtSULTR3.2a/b do not have direct orthologs in Arabidopsis
295 (Figure 2). We preserve the use of SULTR3.2 as a gene name in keeping with convention and refer to this
296 subfamily as SULTR3.1 for now. Phylogenomics-informed gene (re)naming is clearly needed but is beyond
297 the scope of this study (see Tweedie et al. 2025). Our analysis strongly supports four distinct SULTR3 (AC-
298 IIB) subfamilies SULTR3.1, SULTR3.5 (node AC-IIB-1), SULTR3.3, and SULTR3.4 (node AC-IIB-2), alongside
299 the two, well studied AC-IIA subfamilies SULTR1 and SULTR2. Together with the more divergent AC-I
300 SULTR4 group, angiosperm taxa contain seven evolutionarily conserved SULTR subfamilies (Figure 1),
301 rather than the historically proposed four (Takahashi et al. 2000).
302
303 **Exon-intron structure varies with the evolution of *SULTR subfamilies***
304 Analysis of gene structure revealed variations that generally align with the SULTR subfamily evolution
305 inferred from our phylogenetic trees. *SULTR4* genes of the small AC-I clade have 17 exons with
306 evolutionarily conserved junctions among diverse lineages (Figure 3). However, multiple exon-fusion
307 events have occurred in the expanded AC-II subfamilies. Specifically, three fusions between exons 8 and
308 9, exons 10 to 12, and exons 13 and 14 are shared across all AC-II subfamilies and species, including basal
309 spikemoss members (Figure 3). Among them, *Sm184750* (basal to AC-IIB) is likely the founding member
310 with just these three exon fusions. This gene structure is retained in *SULTR1* (AC-IIA), *SULTR3.3* and
311 *SULTR3.4* (AC-IIB-2) members.
312
313 *SULTR2* members (AC-IIA) have an additional fusion between exons 6 and 7. This fusion is absent in the
314 basal Amborella *SULTR2* which retains the same gene structure as the presumed AC-II founding member
315 *Sm184750* and the sister *SULTR1* branch (Figure 3). Interestingly, this fusion is present in the more

316 distantly related spikemoss *Sm169988* basal to AC-IIB (Figure 3). Similarly, the *SULTR3.1* and *SULTR3.5*
317 subfamilies share a conserved fusion of exons 1 and 2 across basal, monocot, and eudicot lineages of the
318 AC-IIB-1 subclade, as well as the less related *Sm113596* basal to AC-IIA (Figure 3). The independent
319 occurrence of the same exon fusion pattern in unrelated lineages may suggest convergent evolution.
320 Alternatively, the minor inconsistencies noted above may reflect limitations in current phylogenetic
321 reconstructions in correctly positioning distant orthologs from early-divergent lineages, such as moss
322 and spikemoss. This limitation is evident for the SULTR4 clade (Figure 1) as previously reported
323 (Takahashi et al. 2012).
324
325 Finally, gene structure analysis also revealed multiple unusual or lineage-specific fusion events. Examples
326 include grass-specific fusions, including secondary fusions between above-mentioned exon fusion
327 events, in *SULTR3.1* and *SULTR3.4* members (Figure 3, Phytozome v13). Furthermore, half of the
328 Arabidopsis *SULTR* family members have unique exon fusion events conserved in Brassicaceae, indicative
329 of their unusual evolution. This suggests that using Arabidopsis genes as sole references for comparative
330 studies may introduce confounding factors for evolutionary inference.
331
332 **Protein modeling reveals binding pocket substitutions in expanded SULTR3 subfamilies**
333 The recently resolved protein structure of Arabidopsis AtSULTR4.1 (Wang et al. 2021) was used as a
334 template to identify key substrate binding residues in other Arabidopsis and poplar SULTR proteins. The
335 key residue Glu347 (AtSULTR4.1 numbering), essential for co-substrate proton sensing and transport, is
336 conserved across all SULTRs (Figure 4A). Key residues lining the sulfate binding pocket, including Gln112,
337 Tyr116, Ser392, and Arg(Lys)393, are also conserved (Figure 4A). Mutations to Ala at any of these
338 positions resulted in a near-total loss of sulfate transport activity (Wang et al. 2021). However, two
339 residues within the predicted binding pocket showed subfamily-specific substitutions. Ala153 is replaced
340 by Ser in SULTR3.3 and SULTR3.4 (node AC-IIB-2), while Ser390 is replaced by Pro in SULTR3.1 and
341 SULTR3.5 (node AC-IIB-1) or by Ala in SULTR3.3 (Figure 4A). Ser390 is thought to interact with Arg393,
342 which likely provides positive electrostatic potential to stabilize substrate binding (Wang et al. 2021).
343 Whether these substitutions contribute to the reported difficulty in demonstrating *in vitro* sulfate
344 transport activity for SULTR3s (Takahashi et al. 2000; Kataoka et al. 2004a) or to the neofunctionalization
345 of SULTR3.4 as SPDT for phosphate transport (Yamaji et al. 2017; Ding et al. 2020) is a possibility that
346 merits consideration.
347

348 To explore this further, we performed AlphaFold3 (Abramson et al. 2024) structural modeling for five
349 representative poplar AC-IIB members: PtaSULTR3.1a, PtaSULTR3.2a, PtaSULTR3.5 (AC-IIB-1),
350 PtaSULTR3.3a, and PtaSULTR3.4a (AC-IIB-2). Structural alignments revealed conserved overall folding
351 across AC-IIB members (Figure 4B). Most models accommodated sulfate ($SO4^{2-}$) and phosphate ($PO4^{3-}$)
352 ions in similar positions (Figure 4C). However, SULTR3.4a displayed a distinct binding mode, with $PO4^{3-}$
353 positioned differently from $SO4^{2-}$, suggesting potential structural selectivity. The Ala→Ser153
354 substitution in AC-IIB-2 introduces a polar hydroxyl group capable of hydrogen bonding. In SULTR3.4a,
355 this residue, along with Ser390 and Ser392, forms a triad of serines that interact with the docked $PO4^{3-}$
356 (Figure 4C), which may help stabilize its higher negative charge (−3). Although SULTR3.3 also contains
357 Ser153, its Ser→Ala390 substitution likely disrupts favorable $PO4^{3-}$ interactions. The other AC-IIB-1
358 SULTR3 members possess only one Ser residue proximal to the substrate, suggesting suboptimal
359 coordination at the binding site (Figure 4C).
360
361 **Expression divergence and tissue partitioning in expanded *SULTR3* subfamilies**
362 We analyzed the expression of poplar *SULTR* genes using published RNA-Seq datasets, including the JGI
363 tissue atlas from *P. tremula* × *P. alba* INRA 717-1B4 (Zhou et al. 2023). The AC-I *PtaSULTR4* transcripts
364 were detected in all tissues, with *PtaSULTR4.1* being higher than *PtaSULTR4.2* in mature leaves and
365 young elongating roots (Figure 5). Among the AC-IIA members, the two *PtaSULTR1.1* paralogs were
366 expressed in all tissues but showed distinct tissue preferences. *PtaSULTR1.1a* transcript levels were
367 highest in the bark and xylem of the primary stem (internodes 3-6), while *PtaSULTR1.1b* transcripts were
368 low overall but predominated in roots (Figure 5). The *PtaSULTR2.1* paralogs were generally poorly
369 expressed, except in primary xylem where *PtaSULTR2.1b* was strongly expressed. *PtaSULTR2.2*, the
370 ancient inverted tandem duplicate of *PtaSULTR1.1b*, was well expressed throughout the plant with a
371 clear bias for mature leaves (Figure 5).
372
373 Members of the expanded AC-IIB subfamilies exhibited substantial expression divergence or partitioning,
374 with many showing restricted tissue distribution. For instance, the singleton *PtaSULTR3.5* was only
375 detected at low levels in buds and roots (Figure 5). No bark expression was detected for the *PtaSULTR3.1*
376 and *PtaSULTR3.5* (AC-IIB-1) subfamilies. *PtaSULTR3.1a* was poorly expressed overall, but the paralogous
377 *PtaSULTR3.1b* was well expressed in both leaves and roots (Figure 5). The *PtaSULTR3.2* pair showed
378 clearly xylem-biased and developmentally conditioned expression in stems. Both genes were expressed
379 in primary xylem, but *PtaSULTR3.2a* expression increased substantially in secondary xylem as

380 *PtaSULTR3.2b* expression sharply decreased (Figure 5). Primary xylem-biased expression was also
381 detected for the *PtaSULTR3.4* paralogs, with *PtaSULTR3.4a* being higher than *PtaSULTR3.4b. PtaSULTR3.3*
382 is the only AC-IIB subfamily that showed broad tissue expression, but this expression was partitioned
383 between the paralogs. *PtaSULTR3.3a* was mainly expressed in stem and root tissues, whereas
384 *PtaSULTR3.3b* was detected in leaves (Figure 5).
385
386 **Differential responses of xylem-biased *SULTR3.2a* and *SULTR3.4a* to drought and lignification**
387 Some *PtaSULTR* genes have previously been shown to be sensitive to seasonal changes in wood or to
388 drought stress in leaves and roots based on qRT-PCR studies (Dürr et al. 2010; Malcheska et al. 2013;
389 Malcheska et al. 2017). Here, we explored data from stress and transgenic perturbation RNA-Seq
390 experiments (Xue et al. 2016; Tsai et al. 2020; Swamy et al. 2015) to analyze *SULTR* expression responses,
391 focusing particularly on vascular tissues and the expanded *SULTR3* subfamilies (excluding *PtaSULTR3.5*
392 which was below detection). We observed a partitioned drought response both between subfamilies and
393 between paralogs, consistent with the partitioned tissue preference discussed above (Figures 5-6). The
394 dominant *PtaSULTR3.1* subfamily members, *PtaSULTR3.1b* and *PtaSULTR3.2a*, were significantly
395 upregulated by drought in roots and secondary xylem, respectively, while their poorly expressed
396 paralogs were unresponsive (Figure 6). Similar patterns were observed for the *PtaSULTR3.3* and
397 *PtaSULTR3.4* subfamilies, with the dominant *PtaSULTR3.3a* and *PtaSULTR3.4a* significantly upregulated in
398 drought-stressed bark and root, respectively. Although both *PtaSULTR3.1b* and *PtaSULTR3.4a* were
399 drought-responsive in root tissue, the expression of *PtaSULTR3.1b* was an order of magnitude higher
400 than that of *PtaSULTR3.4a*. In summary, the data showed that each of the three vascular tissues
401 responded to drought stress by upregulating a distinct AC-IIB (*SULTR3*) subfamily member: *PtaSULTR3.1b*
402 in roots, *PtaSULTR3.2a* in xylem, and *PtaSULTR3.3a* in bark.
403
404 We next examined *SULTR3* expression in the secondary xylem (internodes 60-80) of erect or inclined
405 poplar trees during normal wood (NW) or tension wood (TW) development (Swamy et al. 2015). The
406 secondary xylem-predominant *PtaSULTR3.2a* was down-regulated by more than 70% in TW (Figure 7A).
407 TW in angiosperms is characterized by cellulose-enriched gelatinous fibers with overall reduced lignin
408 accrual (Groover 2016). To further investigate the potential connection between *SULTR3* expression and
409 cell wall composition, we utilized RNA-Seq data from young developing xylem (15 to 30 cm from the
410 shoot tip) of *4CL1* (*4-coumarate:CoA ligase*)-knockout poplar with reduced lignin accumulation (Zhou et
411 al. 2015; Tsai et al. 2020). We observed a 40-50% downregulation of both *PtaSULTR3.2a* and

412 *PtaSULTR3.4a* in the low-lignin *4cl1* mutants (Figure 7B). Interestingly, *PtaSULTR3.4a* transcript
413 abundance was higher than that of *PtaSULTR3.2a*, presumably reflecting the younger stems used in this
414 study compared to the TW experiment (Swamy et al. 2015; Tsai et al. 2020). Together, these results
415 suggest that *PtaSULTR3.2a* expression correlated positively with lignification during stem development,
416 while *PtaSULTR3.4a* response was conditional and limited to primary xylem, where it was most highly
417 expressed (Figures 5 and 7).
418
419 **Gene coexpression of *PtaSULTR3.4a* with phosphorus starvation response and *PtaSULTR3.2a* with**
420 **lignification**
421 To further explore the functional association of the xylem-biased *PtaSULTR3.2a* and *PtaSULTR3.4a*, we
422 performed gene-centered coexpression analysis using 174 published RNA-seq datasets from xylem, bark,
423 and stem tissues (Supplemental Table S2). We identified 419 genes coexpressed with *PtaSULTR3.4a*
424 (Pearson correlation coefficient or PCC ≥ 0.7), which showed significant enrichment in Gene Ontology
425 (GO) terms associated with "cellular response to phosphate starvation", "sulfolipid biosynthetic process",
426 "response to nitrate", "sulfate transport", and "phosphate ion transport" (Figure 8A). Indeed,
427 *PtaSULTR3.4a* was strongly coexpressed with *PtaSULTR3.4b* (PCC = 0.91), *PtaSULTR2.1b* (0.82), and
428 *PtaSULTR2.2* (0.72), as well as genes encoding multiple phosphate transporters (Supplemental Table S3),
429 consistent with previous reports linking the SULTR3.4 subfamily to phosphorus allocation (Yamaji et al.
430 2017; Ding et al. 2020). *PtaSULTR3.4a* was also highly coexpressed with genes known to be sensitive to
431 phosphorus starvation, including orthologs of SPX domain-containing proteins and purple acid
432 phosphatases (Supplemental Table S3) (Duan et al. 2008; Wang et al. 2011; Gan et al. 2015; Chen et al.
433 2022). Our analysis suggests a close coordination of *PtaSULTR3.4a* with a network of transporters and
434 phosphorus responses genes.
435
436 In contrast, a smaller group of 87 genes was coexpressed with *PtaSULTR3.2a*, with significant GO
437 enrichment in "regulation of secondary cell wall biogenesis", "response to wounding", and "secondary
438 metabolic process" (Figure 8A). Specifically, *PtaSULTR3.2* was coexpressed with genes encoding multiple
439 lignin biosynthetic enzymes (phenylalanine ammonia lyase [PAL], cinnamate 4-hydroxylase, 4CLs,
440 hydroxycinnamoyl-CoA shikimate/quinate hydroxycinnamoyl transferase, ferulic acid 5-hydroxylase), C1
441 metabolism enzymes (serine hydroxymethyltransferase [SHMT] and *S*-adenosylmethionine [SAM]
442 synthases), and transcriptional factors regulating secondary wall biogenesis, such as SND (secondary
443 wall-associated NAC domain) and MYB proteins (Zhong et al. 2011) (Supplemental Table S3). We then

444 plotted PCC values for 58 genes involved in lignin biosynthesis, C1 metabolism, and their upstream
445 transcriptional regulators (Supplemental Table S3). We found a median PCC of 0.60 with *PtaSULTR3.2a*
446 but no correlation was observed with *PtaSULTR3.4a* (Figure 8B). Notably, *SULTR3.2a* was positively
447 coexpressed with C1 metabolism genes encoding Met synthases, SAM synthases, homocysteine *S*-
448 methyltransferases, and *S*-adenosylhomocysteine hydrolase of the activated methyl cycle, as well as
449 SHMT and Gly decarboxylase complex enzymes involved in Ser-Gly interconversion (Hanson and Roje
450 2001)(Figure 8B, Supplemental Table S3). For *PAL* and *4CL* gene families involved in both lignin and
451 flavonoid biosynthesis, *PtaSULTR3.2a* coexpression was observed specifically for lignin-associated
452 *PtaPAL2* (Kao et al. 2002), *Pta4CL1* and *Pta4CL5* isoforms (Harding et al. 2002; Tsai et al. 2020)
453 (Supplemental Table S3).
454
455 To further substantiate the link between *SULTR3.2a* and lignification, we mined additional RNA-Seq
456 datasets from transgenic *Populus trichocarpa* with reduced lignin by RNA interference (RNAi) of pathway
457 genes (Wang et al. 2018)(Supplemental Table S4). We confirmed significant down-regulation of
458 *SULTR3.2a* in lignin-reduced transgenic plants, but only for perturbations at the 4CL (consistent with
459 Figure 7B), caffeoyl-CoA *O*-methyltransferase (CCoAOMT), cinnamoyl-CoA reductase (CCR), or caffeic
460 acid *O*-methyltransferase (COMT) steps (Figure 8C). These enzymatic steps involve either CoA-thioester
461 as a co-substrate (4CL) or co-product (CCR) or SAM as a co-factor (CCoAOMT and COMT). Both CoA and
462 SAM are derived from sulfur-containing amino acids (Hanson and Roje 2001; Kupke et al. 2003). In
463 contrast, *SULTR3.4a* was down-regulated in *4CL*-silenced *P. trichocarpa* as in *P. tremula* × *alba* (Figures 7B
464 and 8C), but exhibited variable responses to other lignin gene perturbations, indicative of an indirect
465 connection. Together, independent transgenic experiments in two poplar species and large-scale
466 coexpression analysis all support a previously undescribed link between *SULTR3.2a* and lignification.
467
468
469

470 **DISCUSSION**

471
472 The evolutionary expansion and functional diversification of SULTR transporters from bacteria to higher
473 plants has been extensively discussed (Takahashi et al. 2012). However, important questions remain,
474 especially regarding the large and vascular plant-specific SULTR3 group, whose members exhibit little to

475 no sulfate transport activity on their own (Takahashi et al. 2000; Kataoka et al. 2004a). SULTR3 members
476 exhibit variability in their membrane localization and have been reported to facilitate chloroplast sulfate
477 assimilation, enhance sulfate transport by other SULTR partners, and contribute to phosphorus
478 distribution via the vasculature (Kataoka et al. 2004a; Cao et al. 2013; Zhao et al. 2016; Yamaji et al.
479 2017; Chen et al. 2019; Ding et al. 2020; Gu et al. 2022). By including multiple early-divergent species at
480 key evolutionary junctures for phylogenetic inference, we updated the SULTR family classification into
481 seven distinct subfamilies dating back to basal angiosperms, with four belonging to the enigmatic
482 SULTR3 group. Consistent with experimental evidence from the Arabidopsis, rice, and barley orthologs
483 (Yamaji et al. 2017; Ding et al. 2020; Gu et al. 2022), we provide protein modeling and gene coexpression
484 data supporting the potential neofunctionalization of SULTR3.4 in phosphate homeostasis. We further
485 identified a perennial-specific subgroup within the SULTR3.1 subfamily, with the poplar member
486 *PtaSULTR3.2a* showing strong coexpression with lignin biosynthetic genes and responsiveness to lignin
487 pathway perturbations.
488
489 **Early evolution of seven divergent SULTR subfamilies in angiosperms**
490 Our phylogenetic analysis supports several features of the plant SULTR family evolution previously
491 suggested by Takahashi et al. (2012), based on the placement of moss and spikemoss members. These
492 include the split of AC-I (SULTR4) and AC-II (SULTR1-SULTR3) clades early during land plant evolution, and
493 the subsequent split of AC-IIA (SULTR1-SULTR2) and AC-IIB (SULTR3) subclades, with AC-IIB arising
494 specifically in vascular plants (Figure 1). While AC-IIA is further split into the SULTR1 and SULTR2
495 subfamilies, the much large AC-IIB was previously considered as one (SULTR3) subfamily with four
496 subgroups (Takahashi et al. 2012). However, our phylogenetic reconstruction with basal angiosperm
497 lineages uncovered four strongly supported SULTR3 subfamilies that predate the split of Amborella and
498 tulip tree (Figure 1). Examination of the recently sequenced camphor tree (*Cinnamomum kanehirae* v3)
499 (Chaw et al. 2019) and water lily (*Nymphaea colorata* v1.2)(Zhang et al. 2020) genomes available on
500 Phytozome v13 confirmed the presence of four AC-IIB subfamilies in other early-divergent angiosperm
501 taxa, suggesting their origin in the last common ancestor of all flowering plants.
502
503 Gene structure analysis provided further support for distinct evolution of the AC-IIB subfamilies. It is
504 important to note that gene structure changes, such as intron losses, can impact expression and
505 contribute to functional diversification as effectively, if not more so, than mutations within exons
506 (Morello and Breviario 2008). This was evidenced by preferential yet partitioned expression, both among

507 *SULTR3* subfamilies and between gene duplicates, in vascular tissues of poplar (Figure 5). Drought stress
508 stimulated expression of *PtaSULTR3.1b*, *PtaSULTR3.2a*, and *PtaSULR3.3a* in a root-, xylem-, and bark-
509 biased manner, respectively (Figure 6). These examples serve to illustrate the diverse roles of the four
510 SULTR3 subfamilies beyond the historically established vacuolar (SULTR4), high-affinity (SULTR1), and
511 low-affinity (SULTR2) sulfate transport activities. The four SULTR3 subfamilies likely differentiated as
512 mechanisms for internal distribution and utilization of sulfate evolved in angiosperms (Takahashi 2019).
513
514 **Protein modeling insights into substrate binding pocket sequences**
515 Despite differences in tissue expression and transport kinetics, the proton and sulfate binding pocket
516 residues predicted to be essential for activity (Wang et al. 2021) are conserved in AC-I SULTR4 and AC-IIA
517 SULTR1/SULTR2 subfamilies (Figure 4). However, the expanded AC-IIB (SULTR3) members exhibit
518 subfamily-specific substitutions within the binding pocket, coinciding with reported catalytic divergence.
519 Among AC-IIB members, only SULTR3.1 and SULTR3.5 have been reported to exhibit sulfate uptake
520 activity in yeast, although these findings lack kinetic characterization (Krusell et al. 2005; Xun et al. 2021)
521 and have not been consistently observed across tested species (Takahashi et al. 2000). For instance,
522 Arabidopsis AtSULTR3.5 was found to be nonfunctional by itself but can enhance the activity of
523 AtSULTR2.1 significantly (Kataoka et al. 2004a). Reverse genetics analysis revealed that mutations to
524 AtSULTR3.1 were more detrimental to sulfate uptake by isolated chloroplasts than mutations to any
525 other AC-IIB members (Cao et al. 2013; Chen et al. 2019). Mutations in another SULTR3.1 subfamily
526 member, AtSULTR3.2, has been linked to altered sulfate translocation in developing seeds of Arabidopsis
527 (Zuber et al. 2010). SULTR3.1 and SULTR3.5 differ from the canonical AC-I and AC-IIA subfamilies at
528 position 390 (Pro vs. Ser). Ser390 is thought to interact with Arg393 to stabilize the sulfate ion
529 electrostatically within the binding pocket (Wang et al. 2021). The Ser→Pro390 substitution may impair
530 sulfate ion coordination, potentially contributing to the poor sulfate transport of SULTR3.1 and SULTR3.5
531 (Takahashi et al. 2000; Kataoka et al. 2004a).
532
533 AC-IIB-2 subfamilies SULTR3.3 and SULTR3.4 differ from the other SULTRs at position 153, where Ala is
534 replaced by Ser in the substrate-binding pocket (Figure 4). Furthermore, Ser390 is conserved in SULTR3.4
535 but replaced by Ala in SULTR3.3. In SULT3.4, the three serine residues—Ser153, Ser390, and Ser392—are
536 predicted to enable $PO4^{3-}$ interaction based on protein-substrate modeling (Figure 4). Multiple studies
537 have shown that SULTR3.4 subfamily members transport phosphate rather than sulfate (Yamaji et al.
538 2017; Ding et al. 2020; Gu et al. 2022). Interestingly, phosphate ion coordination in the binding pocket is

539 disrupted in the SULTR3.3 model due to the Ser→Ala390 substitution (Figure 4), consistent with the lack
540 of *in vitro* phosphate or sulfate transport activity reported for rice OsSULTR3.3 (Zhao et al. 2016).
541 However, mutations in *OsSULTR3.3* reduced phytate and total phosphorus concentrations in rice grains
542 (Zhao et al. 2016), suggesting a noncanonical function. Together, these findings highlight unique
543 structural adaptations in SULTR3.4/SPDT that support $PO4^{3-}$ interaction, providing a mechanistic basis
544 for its proposed neofunctionalization in phosphate allocation within the vasculature (Yamaji et al. 2017;
545 Ding et al. 2020). The data also hint at the importance of Ser153 and Ser390 for substrate selectivity.
546 Whether the Pro and Ala substitutions at position 390 contribute to the functional diversification of
547 other SULTR3 subfamilies, either as nonfunctional transporter-like facilitators or through noncanonical
548 roles, remains to be investigated experimentally.
549
550
551 ***PtaSULTR3.4* coexpression with phosphorus transport and starvation response genes**
552 Poplar *PtaSULTR3.4a* and its less expressed genome duplicate *PtaSULTR3.4b* were preferentially
553 expressed in primary xylem. Of the seven Salicoid genome duplicate pairs in the SULTR family,
554 *PtaSULTR3.4s* are the only pair that retains expression conservation in stem vascular tissues. Consistent
555 with a role of the SULTR3.4/SPDT subfamily in phosphorus distribution and metabolism (Yamaji et al.
556 2017; Ding et al. 2020), *PtaSULTR3.4a*-coexpressed genes included several phosphate transporters and
557 phosphate starvation response markers (Gan et al. 2015; Chen et al. 2022). This group also included
558 genes encoding nitrate-responsive regulators, transporters for nitrate, amino acids, auxin, and various
559 metal ions, as well as plasma membrane H^+-ATPases necessary to energize transporters for
560 transmembrane nutrient uptake (Palmgren 2001). The coordinated acquisition of nitrogen and
561 phosphorus, and the crosstalk between nitrate- and phosphorus-responsive signaling pathways have
562 been extensively reported, including in poplar (Gan et al. 2015; Hu and Chu 2020; Ueda et al. 2020). This
563 coordination also extends to other mineral nutrients (Raddatz et al. 2020; Wei et al. 2023). Similarly,
564 sulfur assimilation is sensitive to availability of not only sulfate but also nitrate (Kopriva et al. 2004). Our
565 gene coexpression analysis implicated SULTR3.4 as an important player in these coordinated responses.
566
567 **Secondary xylem-biased *PtaSULTR3.2a* expression and lignification**
568 Extensive prior work has illustrated temporal associations between *SULTR* gene expression and sulfate
569 circulation in poplar stems throughout the year (Rennenberg et al. 2007; Dürr et al. 2010; Malcheska et
570 al. 2013). The sulfate assimilation pathway interfaces with C1 metabolism for the production of SAM,

571 which is a methyl donor for the biosynthesis of lignin and other cell wall polysaccharides (Rajinikanth et
572 al. 2007; Srivastava et al. 2015; Zhang et al. 2019). However, there is little information linking SULTRs
573 with wood formation. A connection was recently suggested via a xylem-expressed microRNA, *miR395c*,
574 which regulated sulfate assimilation genes and low-affinity SULTR2.1b to affect ABA synthesis and
575 secondary cell wall biosynthesis in poplar (Liu et al. 2022).
576
577 In poplar, the AC-IIB-1 member *SULTR3.2a* is the dominant *SULTR* transcript in secondary xylem
578 undergoing secondary cell wall thickening. A functional association between PtaSULTR3.2a and
579 lignification is supported by its reduced expression in low-lignin xylem, either via genetic perturbation in
580 *4cl1* mutants or in TW of trees subjected to stem bending (Figure 7). Significantly lower *SULTR3.2a*
581 expression was also detected in transgenic RNAi *P. trichocarpa* (Wang et al. 2018) targeting 4CL, CCR,
582 CCoAOMT and COMT—enzymatic steps involving sulfur-containing CoA or SAM (Figure 8C). In addition,
583 xylem *PtaSULTR3.2a* expression increased during drought stress, a condition generally associated with
584 enhanced lignification (Moura et al. 2010). We found strong coexpression of *PtaSULTR3.2a* with genes
585 involved in lignin biosynthesis, C1 metabolism, and secondary cell wall biogenesis (Rajinikanth et al.
586 2007; Zhong et al. 2011; Zhang et al. 2019; Donev et al. 2023), accounting for 17% of the 87
587 *PtaSULTR3.2a*-coexpressed genes. While strictly correlative, the conclusion that PtaSULTR3.2a is more
588 closely associated with lignification than other PtaSULTRs is supported by data from a wide range of
589 experimental approaches (Supplemental Table S2), including transgenic perturbation of lignin genes in
590 two distinct species (*P. trichocarpa* of section Tacamahaca and *P. tremula* × *alba* of section *Populus*).
591 Given that PtaSULT3.2a belongs to a small subgroup of the SULTR3.1 subfamily retained only in perennial
592 dicots, its preferential expression in secondary xylem and strong coexpression with lignification genes
593 are consistent with perennial-specific functional diversification.
594
595 In summary, our analysis suggests that the enigmatic SULTR3 contains four distinct subfamilies with an
596 ancient origin predating angiosperm evolution. Variations in exon-intron structure, substrate binding
597 pocket residues, and tissue expression preferences likely contribute to the functional diversification of
598 the four SULTR3 subfamilies. The previously reported neofunctionalization of the SULTR3.4 subfamily
599 associated with phosphorus distribution (Yamaji et al. 2017; Ding et al. 2020; Gu et al. 2022) gained
600 credence in poplar based on structural modeling and coexpression analysis. In addition, we provided
601 evidence supporting the functional diversification of PtaSULTR3.2a associated with lignification in poplar
602 and likely other perennial species. These functional predictions await future experimental verification.

603 Finally, this work highlights the need for phylogeny-informed gene and gene family nomenclatures as
604 discussed elsewhere in this special issue.
605
606 **ACKNOWLEDGEMENTS**
607 The authors thank the advice of Ethan Baldwin and Jim Leebens-Mack on phylogenetic analysis and Ran
608 Zhou on bioinformatics analysis.
609
610 **AUTHORS' CONTRIBUTIONS**
611 C.-J.T. conceived the idea, S.M.S. performed all analyses with assistance from C.H. for RNA-seq and gene
612 coexpression, L.N. performed protein modeling analysis, S.M.S. drafted the manuscript, S.A.H. and C.-J.T.
613 revised the manuscript.
614
615 **SUPPLEMENTARY DATA**
616 Table S1. List of SULTR sequences used in the phylogenetic analysis
617 Table S2. List of RNA-Seq datasets from *Populus tremula* × *alba* stem tissues used in coexpression
618 analysis
619 Table S3. Genes and their Pearson correlation coefficients with *PtaSULTR3.2a* and *PtaSULTR3.4a*
620 Table S4. List of RNA-Seq datasets from transgenic *Populus trichocarpa*
621
622 **FUNDING**
623 The work was supported by the Center for Bioenergy Innovation (CBI), U.S. Department of Energy, Office
624 of Science, Biological and Environmental Research Program under Award Number ERKP886. S.M.S was
625 supported by the Foundation for Food and Agriculture Research fellowship program, C.S. was supported
626 by a Government Scholarship for Overseas Study from the Ministry of Education in Taiwan, and L.N. was
627 supported by the U.S. National Science Foundation under Award Number 2400220.
628
629
630 **CONFLICT OF INTEREST:** None declared.
631
632 **DATA AVAILABILITY STATEMENT**
633 Gene models and genome versions for protein sequences used for phylogenetic analysis are provided in
634 Supplementary Table S1. Accession numbers for RNA-Seq datasets used in gene expression analysis are

SRR6255832 to SRR6255842 for tissue expression, RR1292611, SRR1292615, and SRR1295980-SRR1295983 for stem bending response, SRP041959 for drought response, and PRJNA589632 for lignin perturbation response in *P. tremula* × *alba*. Accession numbers for the 174 RNA-Seq datasets used for gene coexpression analysis are provided in Supplemental Table S2. The accession number for additional RNA-Seq data from lignin-reduced transgenic *P. trichocarpa* is PRJNA314500 and individual sample accession numbers are provided in Supplemental Table S4.

REFERENCES

Abramson, J., J. Adler, J. Dunger, R. Evans, T. Green, A. Pritzel, O. Ronneberger, L. Willmore, A.J. Ballard, J. Bambrick, S.W. Bodenstein, D.A. Evans, C.-C. Hung, M. O'Neill, D. Reiman, K. Tunyasuvunakool, Z. Wu, A. Žemgulytė, E. Arvaniti, C. Beattie, O. Bertolli, A. Bridgland, A. Cherepanov, M. Congreve, A.I. Cowen-Rivers, A. Cowie, M. Figurnov, F.B. Fuchs, H. Gladman, R. Jain, Y.A. Khan, C.M.R. Low, K. Perlin, A. Potapenko, P. Savy, S. Singh, A. Stecula, A. Thillaisundaram, C. Tong, S. Yakneen, E.D. Zhong, M. Zielinski, A. Žídek, V. Bapst, P. Kohli, M. Jaderberg, D. Hassabis and J.M. Jumper. 2024. Accurate structure prediction of biomolecular interactions with AlphaFold 3. Nature. 630:493-500.

Batool, S., V.V. Uslu, H. Rajab, N. Ahmad, R. Waadt, D. Geiger, M. Malagoli, C.B. Xiang, R. Hedrich, H. Rennenberg, C. Herschbach, R. Hell and M. Wirtz. 2018. Sulfate is incorporated into cysteine to trigger ABA production and stomatal closure. Plant Cell. 30:2973-2987.

Bauer, H., P. Ache, S. Lautner, J. Fromm, W. Hartung, Khaled A.S. Al-Rasheid, S. Sonnewald, U. Sonnewald, S. Kneitz, N. Lachmann, Ralf R. Mendel, F. Bittner, Alistair M. Hetherington and R. Hedrich. 2013. The stomatal response to reduced relative humidity requires guard cell-autonomous ABA synthesis. Current Biology. 23:53-57.

Bianchini, G. and P. Sánchez-Baracaldo. 2024. TreeViewer: Flexible, modular software to visualise and manipulate phylogenetic trees. Ecology and Evolution. 14:e10873.

Bray, N.L., H. Pimentel, P. Melsted and L. Pachter. 2016. Near-optimal probabilistic RNA-seq quantification. Nat Biotechnol. 34:525-7.

Cao, M.-J., Z. Wang, M. Wirtz, R. Hell, D.J. Oliver and C.-B. Xiang. 2013. SULTR3;1 is a chloroplast-localized sulfate transporter in Arabidopsis thaliana. The Plant Journal. 73:607-616.

Cao, M.-J., Z. Wang, Q. Zhao, J.-L. Mao, A. Speiser, M. Wirtz, R. Hell, J.-K. Zhu and C.-B. Xiang. 2014. Sulfate availability affects ABA levels and germination response to ABA and salt stress in rabidopsis thaliana. Plant Journal. 77:604-615.

Chaw, S.-M., Y.-C. Liu, Y.-W. Wu, H.-Y. Wang, C.-Y.I. Lin, C.-S. Wu, H.-M. Ke, L.-Y. Chang, C.-Y. Hsu, H.-T. Yang, E. Sudianto, M.-H. Hsu, K.-P. Wu, L.-N. Wang, J.H. Leebens-Mack and I.J. Tsai. 2019. Stout camphor tree genome fills gaps in understanding of flowering plant genome evolution. Nature Plants. 5:63-73.

Chen, N., S. Tong, J. Yang, J. Qin, W. Wang, K. Chen, W. Shi, J. Li, J. Liu and Y. Jiang. 2022. PtoWRKY40 interacts with PtoPHR1-LIKE3 while regulating the phosphate starvation response in poplar. Plant Physiology. 190:2688-2705.

Chen, Y., X. Xiao, R. Yang, Z. Sun, S. Yang, H. Zhang, B. Xing, Y. Li, Q. Liu, Q. Lu, Y. Shi, Y. Yuan, C. Miao and P. Li. 2024. Genome-wide identification and expression-pattern analysis of sulfate transporter

677 (SULTR) gene family in cotton under multiple abiotic stresses and fiber development. Functional
678 & Integrative Genomics. 24:108.
679 Chen, Z., P.X. Zhao, Z.Q. Miao, G.F. Qi, Z. Wang, Y. Yuan, N. Ahmad, M.J. Cao, R. Hell, M. Wirtz and C.B.
680 Xiang. 2019. SULTR3s function in chloroplast sulfate uptake and affect ABA biosynthesis and the
681 stress response. Plant Physiol. 180:593-604.
682 Ding, G., G.J. Lei, N. Yamaji, K. Yokosho, N. Mitani-Ueno, S. Huang and J.F. Ma. 2020. Vascular cambium-
683 localized AtSPDT mediates xylem-to-phloem transfer of phosphorus for its preferential
684 distribution in Arabidopsis. Mol Plant. 13:99-111.
685 Ding, Y., X. Zhou, L. Zuo, H. Wang and D. Yu. 2016. Identification and functional characterization of the
686 sulfate transporter gene GmSULTR1;2b in soybean. BMC Genomics. 17:373.
687 Donev, E.N., M. Derba-Maceluch, Z. Yassin, M.L. Gandla, S. Pramod, E. Heinonen, V. Kumar, G. Scheepers,
688 F. Vilaplana, U. Johansson, M. Hertzberg, B. Sundberg, S. Winestrand, A. Hörnberg, B. Alriksson,
689 L.J. Jönsson and E.J. Mellerowicz. 2023. Field testing of transgenic aspen from large greenhouse
690 screening identifies unexpected winners. Plant Biotechnology Journal. 21:1005-1021.
691 Duan, K., K. Yi, L. Dang, H. Huang, W. Wu and P. Wu. 2008. Characterization of a sub-family of Arabidopsis
692 genes with the SPX domain reveals their diverse functions in plant tolerance to phosphorus
693 starvation. The Plant Journal. 54:965-975.
694 Dürr, J., H. Bücking, S. Mult, H. Wildhagen, K. Palme, H. Rennenberg, F. Ditengou and C. Herschbach.
695 2010. Seasonal and cell type specific expression of sulfate transporters in the phloem of Populus
696 reveals tree specific characteristics for SO(4)(2-) storage and mobilization. Plant Mol Biol. 72:499-
697 517.
698 Ernst, L., J.Q. Goodger, S. Alvarez, E.L. Marsh, B. Berla, E. Lockhart, J. Jung, P. Li, H.J. Bohnert and D.P.
699 Schachtman. 2010. Sulphate as a xylem-borne chemical signal precedes the expression of ABA
700 biosynthetic genes in maize roots. J Exp Bot. 61:3395-405.
701 Ewels, P.A., A. Peltzer, S. Fillinger, H. Patel, J. Alneberg, A. Wilm, M.U. Garcia, P. Di Tommaso and S.
702 Nahnsen. 2020. The nf-core framework for community-curated bioinformatics pipelines. Nature
703 Biotechnology. 38:276-278.
704 Gallardo, K., P.-E. Courty, C. Le Signor, D. Wipf and V. Vernoud. 2014. Sulfate transporters in the plant's
705 response to drought and salinity: regulation and possible functions. Frontiers in Plant Science. 5
706 Gan, H., Y. Jiao, J. Jia, X. Wang, H. Li, W. Shi, C. Peng, A. Polle and Z.-B. Luo. 2015. Phosphorus and
707 nitrogen physiology of two contrasting poplar genotypes when exposed to phosphorus and/or
708 nitrogen starvation. Tree Physiology. 36:22-38.
709 Ge, S.X., D. Jung and R. Yao. 2020. ShinyGO: a graphical gene-set enrichment tool for animals and plants.
710 Bioinformatics. 36:2628-2629.
711 Goodstein, D.M., S. Shu, R. Howson, R. Neupane, R.D. Hayes, J. Fazo, T. Mitros, W. Dirks, U. Hellsten, N.
712 Putnam and D.S. Rokhsar. 2012. Phytozome: a comparative platform for green plant genomics.
713 Nucleic Acids Research. 40:D1178-D1186.
714 Gu, M., H. Huang, H. Hisano, G. Ding, S. Huang, N. Mitani-Ueno, K. Yokosho, K. Sato, N. Yamaji and J.F.
715 Ma. 2022. A crucial role for a node-localized transporter, HvSPDT, in loading phosphorus into
716 barley grains. New Phytologist. 234:1249-1261.
717 Hanson, A.D. and S. Roje. 2001. One-carbon metabolism in higher plants. Annual Review of Plant
718 Physiology and Plant Molecular Biology. 52:119-137.
719 Harding, S.A., J. Leshkevich, V.L. Chiang and C.J. Tsai. 2002. Differential substrate inhibition couples
720 kinetically distinct 4-coumarate:coenzyme A ligases with spatially distinct metabolic roles in
721 quaking aspen. Plant Physiology. 128:428-438.
722 Heidari, P., S. Hasanzadeh, S. Faraji, S. Ercisli and F. Mora-Poblete. 2023. Genome-wide characterization
723 of the sulfate transporter gene family in oilseed crops: *Camelina sativa* and *Brassica napus*.
724 Plants. 12:628.

725 Hu, B. and C. Chu. 2020. Nitrogen–phosphorus interplay: old story with molecular tale. New Phytologist.
726 225:1455-1460.
727 Huang, Q., M. Wang and Z. Xia. 2018. The SULTR gene family in maize (*Zea mays* L.): Gene cloning and
728 expression analyses under sulfate starvation and abiotic stress. Journal of Plant Physiology.
729 220:24-33.
730 Jones, D.T., W.R. Taylor and J.M. Thornton. 1992. The rapid generation of mutation data matrices from
731 protein sequences. Comput Appl Biosci. 8:275-82.
732 Kalyaanamoorthy, S., B.Q. Minh, T.K.F. Wong, A. von Haeseler and L.S. Jermiin. 2017. ModelFinder: fast
733 model selection for accurate phylogenetic estimates. Nature Methods. 14:587-589.
734 Kao, Y.Y., S.A. Harding and C.J. Tsai. 2002. Differential expression of two distinct phenylalanine ammonia-
735 lyase genes in condensed tannin-accumulating and lignifying cells of quaking aspen. Plant
736 Physiology. 130:796-807.
737 Kataoka, T., N. Hayashi, T. Yamaya and H. Takahashi. 2004a. Root-to-shoot transport of sulfate in
738 Arabidopsis. Evidence for the role of SULTR3;5 as a component of low-affinity sulfate transport
739 system in the root vasculature. Plant Physiol. 136:4198-204.
740 Kataoka, T., A. Watanabe-Takahashi, N. Hayashi, M. Ohnishi, T. Mimura, P. Buchner, M.J. Hawkesford, T.
741 Yamaya and H. Takahashi. 2004b. Vacuolar sulfate transporters are essential determinants
742 controlling internal distribution of sulfate in Arabidopsis. Plant Cell. 16:2693-704.
743 Ko, J.-H., C. Prassinos, D. Keathley, K.-H. Han and C. Li. 2011. Novel aspects of transcriptional regulation in
744 the winter survival and maintenance mechanism of poplar. Tree Physiology. 31:208-225.
745 Kopriva, S., T. Hartmann, G. Massaro, P. Hönicke and H. Rennenberg. 2004. Regulation of sulfate
746 assimilation by nitrogen and sulfur nutrition in poplar trees. Trees. 18:320-326.
747 Kopriva, S., M. Malagoli and H. Takahashi. 2019. Sulfur nutrition: impacts on plant development,
748 metabolism, and stress responses. Journal of Experimental Botany. 70:4069-4073.
749 Krusell, L., K. Krause, T. Ott, G. Desbrosses, U. Krämer, S. Sato, Y. Nakamura, S. Tabata, E.K. James, N.
750 Sandal, J. Stougaard, M. Kawaguchi, A. Miyamoto, N. Suganuma and M.K. Udvardi. 2005. The
751 sulfate transporter SST1 is crucial for symbiotic nitrogen fixation in Lotus japonicus root nodules.
752 Plant Cell. 17:1625-36.
753 Kumar, S., G. Stecher, M. Li, C. Knyaz and K. Tamura. 2018. MEGA X: Molecular Evolutionary Genetics
754 Analysis across Computing Platforms. Molecular Biology and Evolution. 35:1547-1549.
755 Kupke, T., P. Hernández-Acosta and F.A. Culiáñez-Macià. 2003. 4'-Phosphopantetheine and coenzyme a
756 biosynthesis in plants. Journal of Biological Chemistry. 278:38229-38237.
757 Liu, C., D. Ma, Z. Wang, N. Chen, X. Ma and X.-Q. He. 2022. MiR395c regulates secondary xylem
758 development through sulfate metabolism in poplar. Frontiers in Plant Science. 13
759 Madeira, F., N. Madhusoodanan, J. Lee, A. Eusebi, A. Niewielska, A.R.N. Tivey, S. Meacham, R. Lopez and
760 S. Butcher. 2024. Using EMBL-EBI Services via Web Interface and Programmatically via Web
761 Services. Current Protocols. 4:e1065.
762 Malcheska, F., A. Ahmad, S. Batool, H.M. Müller, J. Ludwig-Müller, J. Kreuzwieser, D. Randewig, R.
763 Hänsch, R.R. Mendel, R. Hell, M. Wirtz, D. Geiger, P. Ache, R. Hedrich, C. Herschbach and H.
764 Rennenberg. 2017. Drought-enhanced xylem sap sulfate closes stomata by affecting ALMT12 and
765 guard cell ABA synthesis. Plant Physiol. 174:798-814.
766 Malcheska, F., A. Honsel, H. Wildhagen, J. Dürr, C. Larisch, H. Rennenberg and C. Herschbach. 2013.
767 Differential expression of specific sulphate transporters underlies seasonal and spatial patterns
768 of sulphate allocation in trees. Plant, Cell & Environment. 36:1285-1295.
769 Martin, M. 2011. Cutadapt removes adapter sequences from high-throughput sequencing reads. 2011.
770 17:3.
771 Maruyama-Nakashita, A., A. Watanabe-Takahashi, E. Inoue, T. Yamaya, K. Saito and H. Takahashi. 2015.
772 Sulfur-responsive elements in the 3′-nontranscribed intergenic region are essential for the

773 induction of SULFATE TRANSPORTER 2;1 gene expression in arabidopsis roots under sulfur
774 deficiency. Plant Cell. 27:1279-1296.
775 Morello, L. and D. Breviario. 2008. Plant spliceosomal introns: not only cut and paste. Curr Genomics.
776 9:227-38.
777 Moura, J.C.M.S., C.A.V. Bonine, J.D.O.F. Viana, M.C. Dornelas and P. Mazzafera. 2010. Abiotic and biotic
778 stresses and changes in the lignin content and composition in plants. Journal of Integrative Plant
779 Biology. 52:360-376.
780 Nguyen, L.T., H.A. Schmidt, A. von Haeseler and B.Q. Minh. 2015. IQ-TREE: a fast and effective stochastic
781 algorithm for estimating maximum-likelihood phylogenies. Mol Biol Evol. 32:268-74.
782 Notredame, C., D.G. Higgins and J. Heringa. 2000. T-Coffee: A novel method for fast and accurate
783 multiple sequence alignment. J Mol Biol. 302:205-17.
784 Palmgren, M.G. 2001. PLANT PLASMA MEMBRANE H+-ATPases: Powerhouses for Nutrient Uptake.
785 Annual Review of Plant Biology. 52:817-845.
786 Pfautsch, S., T. Hölttä and M. Mencuccini. 2015. Hydraulic functioning of tree stems—fusing ray anatomy,
787 radial transfer and capacitance. Tree Physiology. 35:706-722.
788 Puresmaeli, F., P. Heidari and S. Lawson. 2023. Insights into the sulfate transporter gene family and its
789 expression patterns in durum wheat seedlings under salinity. Genes. 14:333.
790 Raddatz, N., L. Morales de los Ríos, M. Lindahl, F.J. Quintero and J.M. Pardo. 2020. Coordinated Transport
791 of Nitrate, Potassium, and Sodium. Frontiers in Plant Science. 11
792 Rajinikanth, M., S.A. Harding and C.-J. Tsai. 2007. The glycine decarboxylase complex multienzyme family
793 in Populus. Journal of Experimental Botany. 58:1761-1770.
794 Rennenberg, H., C. Herschbach, K. Haberer and S. Kopriva. 2007. Sulfur metabolism in plants: Are trees
795 different? Plant Biology. 9:620-637.
796 Rouached, H., M. Wirtz, R. Alary, R.d. Hell, A.B. Arpat, J.-C. Davidian, P. Fourcroy and P. Berthomieu.
797 2008. Differential regulation of the expression of two high-affinity sulfate transporters, SULTR1.1
798 and SULTR1.2, in *Arabidopsis* Plant Physiology. 147:897-911.
799 Srivastava, A.C., F. Chen, T. Ray, S. Pattathil, M.J. Peña, U. Avci, H. Li, D.V. Huhman, J. Backe, B.
800 Urbanowicz, J.S. Miller, M. Bedair, C.E. Wyman, L.W. Sumner, W.S. York, M.G. Hahn, R.A. Dixon,
801 E.B. Blancaflor and Y. Tang. 2015. Loss of function of folylpolyglutamate synthetase 1 reduces
802 lignin content and improves cell wall digestibility in Arabidopsis. Biotechnology for Biofuels.
803 8:224.
804 Swamy, P.S., H. Hu, S. Pattathil, V.J. Maloney, H. Xiao, L.-J. Xue, J.-D. Chung, V.E. Johnson, Y. Zhu, G.F.
805 Peter, M.G. Hahn, S.D. Mansfield, S.A. Harding and C.-J. Tsai. 2015. Tubulin perturbation leads to
806 unexpected cell wall modifications and affects stomatal behaviour in Populus. Journal of
807 Experimental Botany. 66:6507-6518.
808 Takahashi, H. 2019. Sulfate transport systems in plants: functional diversity and molecular mechanisms
809 underlying regulatory coordination. Journal of Experimental Botany. 70:4075-4087.
810 Takahashi, H., P. Buchner, N. Yoshimoto, M.J. Hawkesford and S.-H. Shiu. 2012. Evolutionary relationships
811 and functional diversity of plant sulfate transporters. Frontiers in Plant Science. 2
812 Takahashi, H., A. Watanabe-Takahashi, F.W. Smith, M. Blake-Kalff, M.J. Hawkesford and K. Saito. 2000.
813 The roles of three functional sulphate transporters involved in uptake and translocation of
814 sulphate in Arabidopsis thaliana. The Plant Journal. 23:171-182.
815 Takahashi, H., M. Yamazaki, N. Sasakura, A. Watanabe, T. Leustek, J.A. Engler, G. Engler, M. Van Montagu
816 and K. Saito. 1997. Regulation of sulfur assimilation in higher plants: a sulfate transporter
817 induced in sulfate-starved roots plays a central role in Arabidopsis thaliana. Proc Natl Acad Sci U
818 S A. 94:11102-7.
819 Tsai, C.-J., P. Xu, L.-J. Xue, H. Hu, B. Nyamdari, R. Naran, X. Zhou, G. Goeminne, R. Gao, E. Gjersing, J.
820 Dahlen, S. Pattathil, M.G. Hahn, M. Davis, J. Ralph, W.A. Boerjan and S.A. Harding. 2020.

821 Compensatory guaiacyl lignin biosynthesis at the expense of syringyl lignin in *4CL1*-knockout
822 poplar. Plant Physiology. 183:123-136.
823 Tweedie, S., S. Martin and E. Bruford. 2025. Towards an official gene nomenclature for Populus
824 trichocarpa. Tree Physiology
825 Ueda, Y., T. Kiba and S. Yanagisawa. 2020. Nitrate-inducible NIGT1 proteins modulate phosphate uptake
826 and starvation signalling via transcriptional regulation of SPX genes. Plant Journal. 102:448-466.
827 Vidmar, J.J., J.K. Schjoerring, B. Touraine and A.D.M. Glass. 1999. Regulation of the hvst1 gene encoding a
828 high-affinity sulfate transporter from Hordeum vulgare. Plant Molecular Biology. 40:883-892.
829 Wang, J.P., M.L. Matthews, C.M. Williams, R. Shi, C. Yang, S. Tunlaya-Anukit, H.-C. Chen, Q. Li, J. Liu, C.-Y.
830 Lin, P. Naik, Y.-H. Sun, P.L. Loziuk, T.-F. Yeh, H. Kim, E. Gjersing, T. Shollenberger, C.M. Shuford, J.
831 Song, Z. Miller, Y.-Y. Huang, C.W. Edmunds, B. Liu, Y. Sun, Y.-C.J. Lin, W. Li, H. Chen, I. Peszlen, J.J.
832 Ducoste, J. Ralph, H.-M. Chang, D.C. Muddiman, M.F. Davis, C. Smith, F. Isik, R. Sederoff and V.L.
833 Chiang. 2018. Improving wood properties for wood utilization through multi-omics integration in
834 lignin biosynthesis. Nature Communications. 9:1579.
835 Wang, L., K. Chen and M. Zhou. 2021. Structure and function of an Arabidopsis thaliana sulfate
836 transporter. Nature Communications. 12:4455.
837 Wang, L., Z. Li, W. Qian, W. Guo, X. Gao, L. Huang, H. Wang, H. Zhu, J.W. Wu, D. Wang and D. Liu. 2011.
838 The Arabidopsis purple acid phosphatase AtPAP10 is predominantly associated with the root
839 surface and plays an important role in plant tolerance to phosphate limitation. Plant Physiol.
840 157:1283-99.
841 Wei, M., M. Zhang, J. Sun, Y. Zhao, S. Pak, M. Ma, Y. Chen, H. Lu, J. Yang, H. Wei, Y. Li and C. Li. 2023.
842 PuHox52 promotes coordinated uptake of nitrate, phosphate, and iron under nitrogen deficiency
843 in Populus ussuriensis. J Integr Plant Biol. 65:791-809.
844 Xue, L.-J., C.J. Frost, C.-J. Tsai and S.A. Harding. 2016. Drought response transcriptomics are altered in
845 poplar with reduced tonoplast sucrose transporter expression. Scientific Reports. 6:33655.
846 Xun, M., J. Song, J. Shi, J. Li, Y. Shi, J. Yan, W. Zhang and H. Yang. 2021. Genome-wide identification of
847 sultr genes in *Malus domestica* and low sulfur-induced MhSultr3;1a to increase cysteine-
848 improving growth. Frontiers in Plant Science. 12
849 Yamaji, N., Y. Takemoto, T. Miyaji, N. Mitani-Ueno, K.T. Yoshida and J.F. Ma. 2017. Reducing phosphorus
850 accumulation in rice grains with an impaired transporter in the node. Nature. 541:92-95.
851 Yoshimoto, N., H. Takahashi, F.W. Smith, T. Yamaya and K. Saito. 2002. Two distinct high-affinity sulfate
852 transporters with different inducibilities mediate uptake of sulfate in Arabidopsis roots. Plant
853 Journal. 29:465-473.
854 Zhang, J., M. Li, A.C. Bryan, C.G. Yoo, W. Rottmann, K.A. Winkeler, Cassandra M. Collins, V. Singan, E.A.
855 Lindquist, S.S. Jawdy, L.E. Gunter, N.L. Engle, X. Yang, K. Barry, T.J. Tschaplinski, J. Schmutz, Y. Pu,
856 A.J. Ragauskas, G.A. Tuskan, W. Muchero and J.-G. Chen. 2019. Overexpression of a serine
857 hydroxymethyltransferase increases biomass production and reduces recalcitrance in the
858 bioenergy crop Populus. Sustainable Energy & Fuels. 3:195-207.
859 Zhang, L., F. Chen, X. Zhang, Z. Li, Y. Zhao, R. Lohaus, X. Chang, W. Dong, S.Y.W. Ho, X. Liu, A. Song, J. Chen,
860 W. Guo, Z. Wang, Y. Zhuang, H. Wang, X. Chen, J. Hu, Y. Liu, Y. Qin, K. Wang, S. Dong, Y. Liu, S.
861 Zhang, X. Yu, Q. Wu, L. Wang, X. Yan, Y. Jiao, H. Kong, X. Zhou, C. Yu, Y. Chen, F. Li, J. Wang, W.
862 Chen, X. Chen, Q. Jia, C. Zhang, Y. Jiang, W. Zhang, G. Liu, J. Fu, F. Chen, H. Ma, Y. Van de Peer and
863 H. Tang. 2020. The water lily genome and the early evolution of flowering plants. Nature.
864 577:79-84.
865 Zhao, H., T. Frank, Y. Tan, C. Zhou, M. Jabnoune, A.B. Arpat, H. Cui, J. Huang, Z. He, Y. Poirier, K.-H. Engel
866 and Q. Shu. 2016. Disruption of Os3;3 reduces phytate and phosphorus concentrations and
867 alters the metabolite profile in rice grains. New Phytologist. 211:926-939.

868 Zhao, Q., J. Geng, Y. Du, S. Li, X. Yuan, J. Zhu, Z. Zhou, Q. Wang and J. Du. 2022. The common bean
869 (*Phaseolus vulgaris*) SULTR gene family: genome-wide identification, phylogeny, evolutionary
870 expansion and expression patterns. Biotechnology & Biotechnological Equipment. 36:724-736.
871 Zhong, R., R.L. McCarthy, C. Lee and Z.-H. Ye. 2011. Dissection of the transcriptional program regulating
872 secondary wall biosynthesis during wood formation in poplar. Plant Physiology. 157:1452-1468.
873 Zhou, J., Y. Dong, Y. Liu, Y. Huang, W. Jiang, X. Zheng, H. Zhang, N. Gong and X. Bai. 2024. Identification
874 and expression analysis of sulfate transporter genes family and function analysis of
875 GmSULTR3;1a from soybean. Int J Mol Sci. 25
876 Zhou, R., J.W. Jenkins, Y. Zeng, S. Shu, H. Jang, S.A. Harding, M. Williams, C. Plott, K.W. Barry, M.
877 Koriabine, M. Amirebrahimi, J. Talag, S. Rajasekar, J. Grimwood, R.J. Schmitz, R.K. Dawe, J.
878 Schmutz and C.-J. Tsai. 2023. Haplotype-resolved genome assembly of *Populus tremula* × *P. alba*
879 reveals aspen-specific megabase satellite DNA. Plant Journal. 16:1003-1017.
880 Zhou, X., T.B. Jacobs, L.-J. Xue, S.A. Harding and C.-J. Tsai. 2015. Exploiting SNPs for biallelic CRISPR
881 mutations in the outcrossing woody perennial *Populus* reveals 4-coumarate:CoA ligase specificity
882 and redundancy. New Phytologist. 208:298-301.
883 Zuber, H., J.C. Davidian, G. Aubert, D. Aimé, M. Belghazi, R. Lugan, D. Heintz, M. Wirtz, R. Hell, R.
884 Thompson and K. Gallardo. 2010. The seed composition of Arabidopsis mutants for the group 3
885 sulfate transporters indicates a role in sulfate translocation within developing seeds. Plant
886 Physiol. 154:913-26.

887

888 **FIGURE LEGENDS**

889 **Figure 1.** Maximum likelihood phylogenetic inference of 262 SULTR sequences from 22 plant genomes.
890 Angiosperm SULTRs form two ancient clades, AC-I and AC-II. The AC-I clade represents the SULTR4
891 subfamily. The AC-II clade consists of two subclades, with AC-IIA represented by the SULTR1 and SULTR2
892 subfamilies, and AC-IIB by SULTR3. AC-IIB is present exclusively in vascular plants with four well-
893 supported groups organized into two branches in all angiosperm taxa. The AC-IIB-1 branch contains
894 SULTR3.1 and SULTR3.5 subfamilies, whereas AC-IIB-2 includes SULTR3.3 and SULTR3.4 subfamilies.
895 Bootstrap values for major nodes are shown.

896 **Figure 2.** Maximum likelihood phylogenetic inference of AC-IIB members from 20 angiosperm genomes.
897 The 125 angiosperm SULTR3 members form two branches each with two nodes, rooted on the two
898 *Selaginella moellendorffi* sequences. The four color-coded nodes represent SULTR3.1 and SULTR3.5 of
899 AC-IIB-1, and SULTR3.3 and SULTR3.4 of AC-IIB-2. The perennial-specific subgroup within the SULTR3.1
900 subfamily is highlighted in darker shade. Bootstrap values for major nodes are shown.

901 **Figure 3.** Exon-intron structures of *SULTR* genes of nine representative species. Genes are arranged by
902 phylogenetic classification, with basal lineages shown on top of each group. Conserved exon fusion
903 events are colored and gray denotes lineage-specific fusion events. Introns are not drawn to scale and

904 first exons are trimmed for alignments. Boldface indicates perennial-specific SULTR3.1 subfamily
905 members.

906 **Figure 4.** Sequence and structural comparisons of SULTR members. **A**, Sequence alignments of
907 *Arabidopsis thaliana* and *Populus trichocarpa* SULTRs near the predicted substrate-binding pocket.
908 Amino acid residue numbering follows the structure-resolved AtSULTR4.1 (AT5G13550), shown at the
909 top. Other sequences are arranged by phylogenetic grouping. Boldface indicates perennial-specific
910 SULTR3.1 subfamily members. Green- and purple-shaded positions denote residues critical to proton and
911 sulfate binding or interaction, respectively. **B**, Structure alignment of AlphaFold3 models of PtaSULTR3.1a
912 (yellow), PtaSULTR3.2a (purple), PtaSULTR3.3a (blue), PtaSULTR3.4a (green), and PtaSULTR3.5 (grey)
913 showing overall fold conservation. The dotted circle denotes the substrate-binding site. **C**, Close-up views
914 of the substrate-binding pockets docked with sulfate ($SO4^{2-}$, red spheres, top row) or phosphate (PO_4^{3-},
915 blue spheres, bottom row). Key residues are highlighted, with AtSULTR4 numbering shown in
916 parentheses.

917 **Figure 5.** Heatmap illustration of *SULTR* gene expression across *Populus* tissues. Genes are arranged by
918 phylogenetic grouping and genome duplicates are denoted as a and b. Boldface indicates perennial-
919 specific SULTR3.1 subfamily members. Data were from JGI tissue atlas of Zhou et al. 2023.

920 **Figure 6.** Drought stress response of *Populus SULTR3* members. The four *SULTR3* subfamilies showed
921 partitioned tissue response to drought stress, with divergent expression strengths between genome
922 duplicates. Bars are means ± SE of n = 3 biological replicates. Significance testing was conducted using
923 the two-sample *t*-test against well-watered samples (**, $P \leq 0.01$; * $P \leq 0.05$). Data were from Xue et al.
924 2016.

925 **Figure 7.** Xylem expression responses of *Populus SULTR3* members to genetic or environmental
926 perturbations. **A**, Transcript abundance in normal wood (NW) versus tension wood (TW) from *P. tremula*
927 × *alba* stem internodes 60-80 (Swamy et al. 2015). **B,** Transcript abundance in *P. tremula* × *alba* control
928 versus lignin-reduced *4cl1* xylem of young stem internodes 15-30 cm from the shoot tip (Tsai et al. 2020).
929 Bars are means ± SE of n = 3 biological replicates. Statistical significance was assessed using two-sample
930 *t*-test (***, $P \leq 0.001$; **, $P \leq 0.01$; * $P \leq 0.05$).

931 **Figure 8.** Gene-centered coexpression analysis of xylem-biased *PtaSULT3.2a* and *PtaSULTR3.4a*. **A,** GO
932 enrichment of 87 and 419 genes co-expressed (Pearson correlation coefficient [PCC] ≥ 0.7) with
933 *PtaSULT3.2a* and *PtaSULTR3.4a*, respectively, across 174 published *P. tremula* × *alba* RNA-seq datasets

934 from stem vascular tissues. **B,** Boxplot distribution of PCC values against 58 genes annotated and color-
935 coded for their involvement in lignin biosynthesis, C1 metabolism, and upstream transcription factors
936 (TFs). The gene list is provided in Supplemental Table S3. **C**, Heatmap depictions of lignin content
937 differentials and expression fold changes of *SULTR3.2a* and *SULTR3.4a* in transgenic *P. trichocarpa* with
938 downregulated lignin biosynthetic genes (Wang et al. 2018). Statistical significance was determined using
939 two-sample *t*-test (boldfaced, $P \leq .01$; italic-underlined, $P \leq .05$).

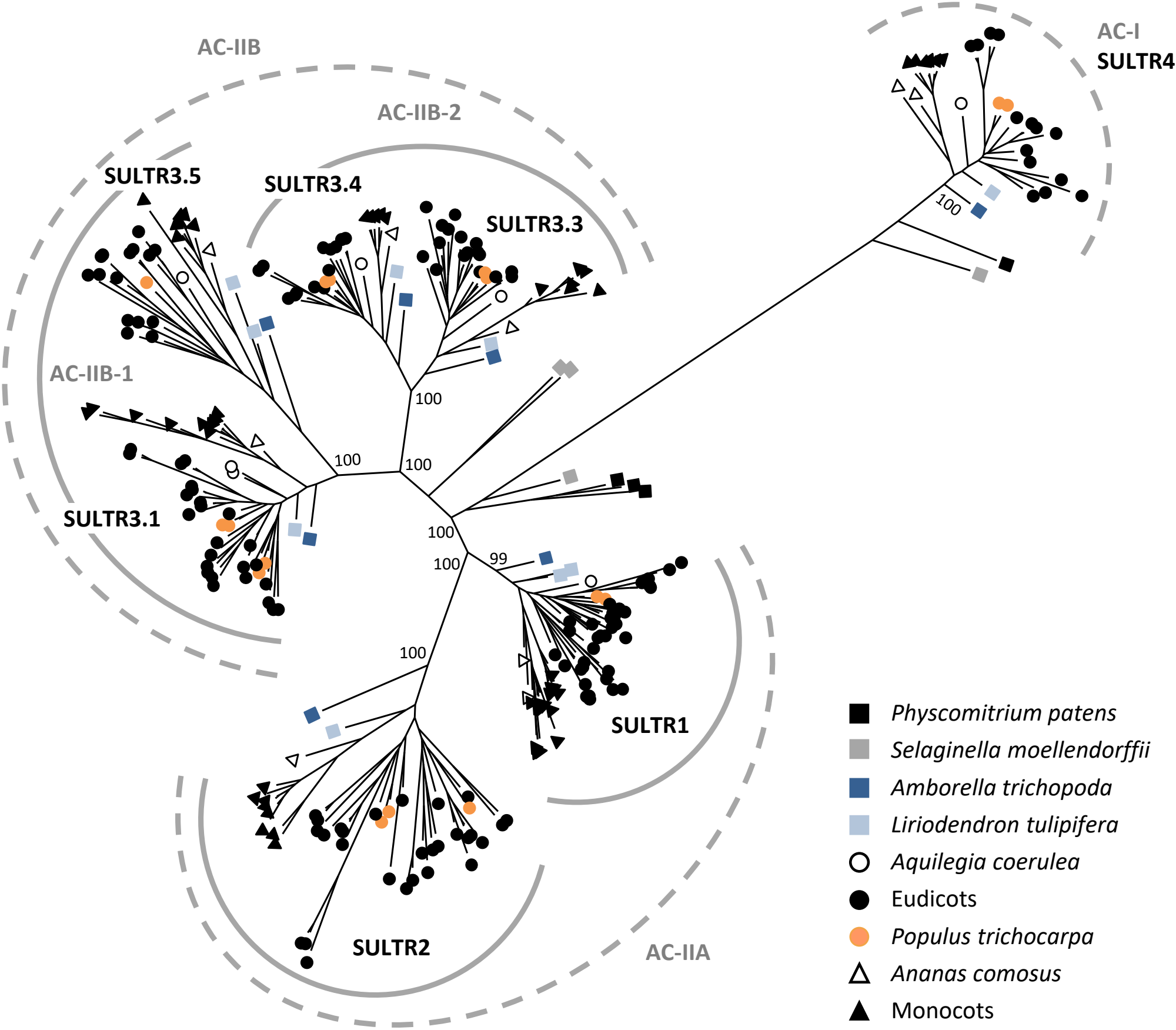
AC-IIB
AC-IIB-2
AC-IIB-1
AC-I
AC-IIA
SULTR3.5
SULTR3.4
SULTR3.3
SULTR3.1
SULTR4
SULTR1
SULTR2
100
100
100
100
100
100
99
100
Physcomitrium patens
Selaginella moellendorffii
Amborella trichopoda
Liriodendron tulipifera
Aquilegia coerulea
Eudicots
Populus trichocarpa
Ananas comosus
Monocots

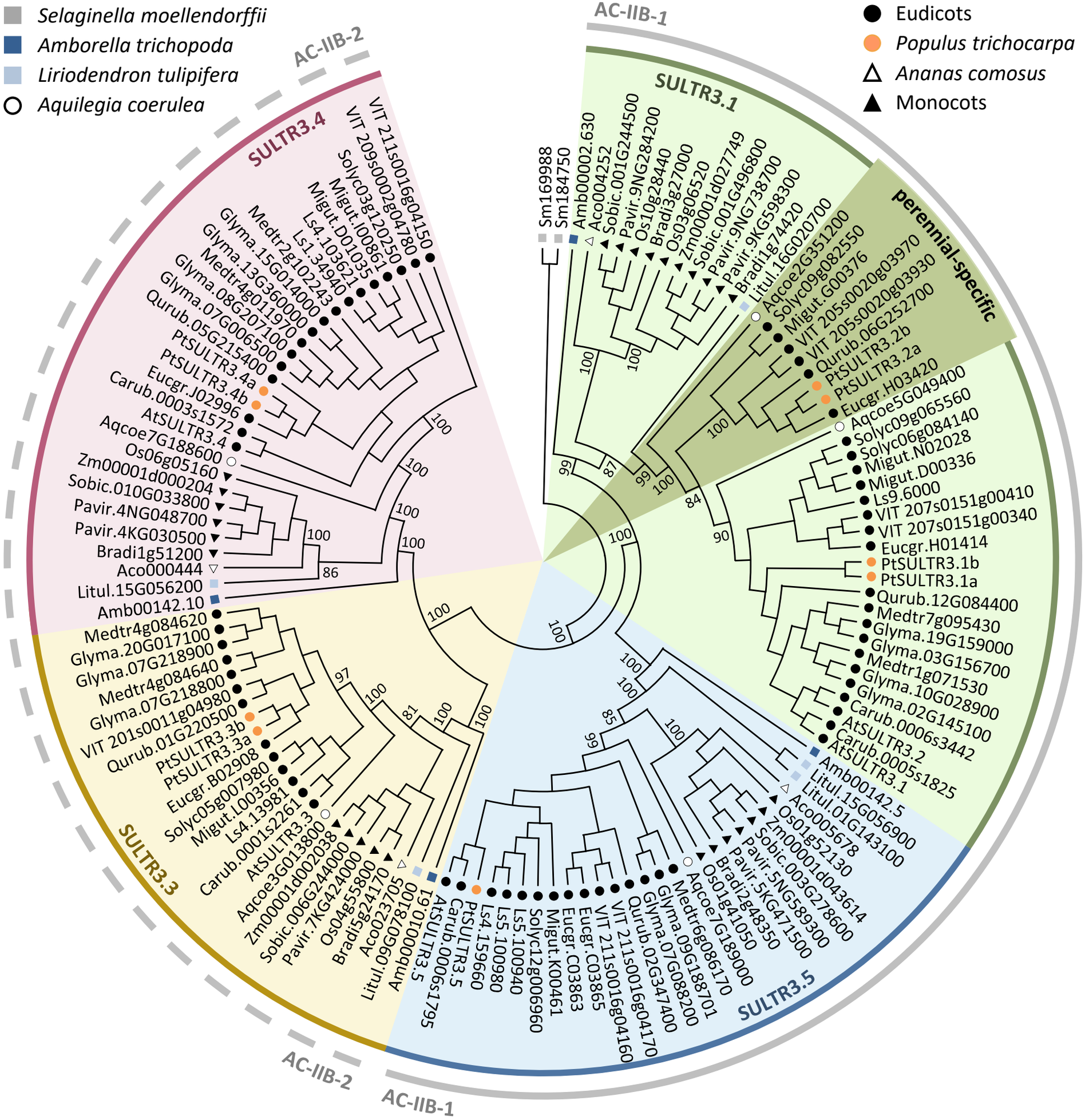
Selaginella moellendorffii
Amborella trichopoda
Liriodendron tulipifera
Aquilegia coerulea
Eudicots
Populus trichocarpa
Ananas comosus
Monocots
AC-IIB-1
AC-IIB-2
SULTR3.1
SULTR3.2
SULTR3.3
SULTR3.4
SULTR3.5
perennial-specific
Sm169988
Sm184750
Amb00002.630
Aco004252
Sobic.001G244500
Pavir.9NG284200
Os10g28440
Bradi3g27000
Os03g06520
Zm00001d027749
Sobic.001G496800
Pavir.9KG598300
Bradi1g74420
Litul.16G020700
Aqcoe2G351200
Solyc09g082550
Migut.G00376
VIT 205s0020g03970
VIT 205s0020g03930
Qurub.06G252700
PtSULTR3.2b
PtSULTR3.2a
Eucgr.H03420
Aqcoe5G049400
Solyc09g065560
Solyc06g084140
Migut.N02028
Migut.D00336
Ls9.6000
VIT 207s0151g00410
VIT 207s0151g00340
Eucgr.H01414
PtSULTR3.1b
PtSULTR3.1a
Qurub.12G084400
Medtr7g095430
Glyma.19G159000
Glyma.03G156700
Medtr1g071530
Glyma.10G028900
Glyma.02G145100
Carub.0006s3442
AtSULTR3.2
Carub.0005s1825
AtSULTR3.1
Amb00142.5
Litul.15G056900
Litul.01G143100
Aco005678
Os01g52130
Zm00001d043614
Sobic.003G278600
Pavir.5NG589300
Pavir.5KG471500
Bradi2g48350
Os01g41050
Aqcoe7G189000
Medtr6g086170
Glyma.09G188701
Glyma.07G088200
Qurub.02G347400
VIT 211s0016g04170
VIT 211s0016g04160
Eucgr.C03865
Eucgr.C03863
Migut.K00461
Solyc12g006960
Ls5.100940
Ls5.100980
Ls4.159660
PtSULTR3.5
Carub.0006s1795
AtSULTR3.5
Amb00010.61
Litul.09G078100
Aco023705
Bradi5g24170
Os04g55800
Pavir.7KG424000
Sobic.006G244000
Zm00001d002038
Aqcoe3G013800
AtSULTR3.3
Carub.0001s2261
Ls4.13981
Migut.L00356
Solyc05g007980
Eucgr.B02908
PtSULTR3.3a
PtSULTR3.3b
Qurub.01G220500
VIT 201s0011g04980
Glyma.07G218800
Medtr4g084640
Glyma.07G218900
Glyma.20G017100
Medtr4g084620
Amb00142.10
Litul.15G056200
Aco000444
Bradi1g51200
Pavir.4KG030500
Pavir.4NG048700
Sobic.010G033800
Zm00001d000204
Os06g05160
Aqcoe7G188600
AtSULTR3.4
Carub.0003s1572
Eucgr.J02996
PtSULTR3.4b
PtSULTR3.4a
PtSULTR3.5
Qurub.05G215400
Glyma.07G006500
Medtr4g011970
Glyma.08G207100
Glyma.13G360000
Glyma.15G014000
Medtr2g102243
Ls1.34940
Ls4.103621
Migut.D01035
Migut.I00861
Solyc03g120250
VIT 209s0002g04780
VIT 211s0016g04150

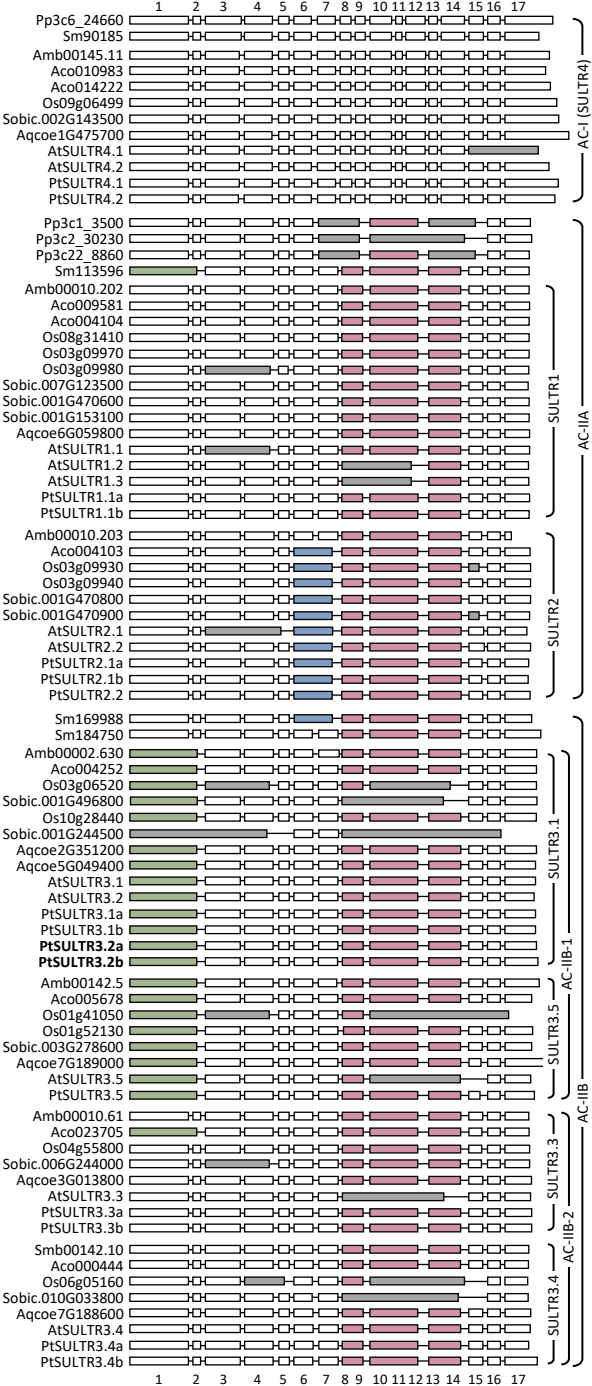
1 2 3 4 5 6 7 8 9 10 11 12 13 14 15 16 17
Pp3c6_24660
Sm90185
Amb00145.11
Aco010983
Aco014222
Os09g06499
Sobic.002G143500
Aqcoe1G475700
AtSULTR4.1
AtSULTR4.2
PtSULTR4.1
PtSULTR4.2
AC-I (SULTR4)
Pp3c1_3500
Pp3c2_30230
Pp3c22_8860
Sm113596
Amb00010.202
Aco009581
Aco004104
Os08g31410
Os03g09970
Os03g09980
Sobic.007G123500
Sobic.001G470600
Sobic.001G153100
Aqcoe6G059800
AtSULTR1.1
AtSULTR1.2
AtSULTR1.3
PtSULTR1.1a
PtSULTR1.1b
SULTR1
Amb00010.203
Aco004103
Os03g09930
Os03g09940
Sobic.001G470800
Sobic.001G470900
AtSULTR2.1
AtSULTR2.2
PtSULTR2.1a
PtSULTR2.1b
PtSULTR2.2
SULTR2
AC-IIA
Sm169988
Sm184750
Amb00002.630
Aco004252
Os03g06520
Sobic.001G496800
Os10g28440
Sobic.001G244500
Aqcoe2G351200
Aqcoe5G049400
AtSULTR3.1
AtSULTR3.2
PtSULTR3.1a
PtSULTR3.1b
PtSULTR3.2a
PtSULTR3.2b
SULTR3.1
Amb00142.5
Aco005678
Os01g41050
Os01g52130
Sobic.003G278600
Aqcoe7G189000
AtSULTR3.5
PtSULTR3.5
SULTR3.5
AC-IIB-1
Amb00010.61
Aco023705
Os04g55800
Sobic.006G244000
Aqcoe3G013800
AtSULTR3.3
PtSULTR3.3a
PtSULTR3.3b
SULTR3.3
Smb00142.10
Aco000444
Os06g05160
Sobic.010G033800
Aqcoe7G188600
AtSULTR3.4
PtSULTR3.4a
PtSULTR3.4b
SULTR3.4
AC-IIB-2
AC-IIB
1 2 3 4 5 6 7 8 9 10 11 12 13 14 15 16 17

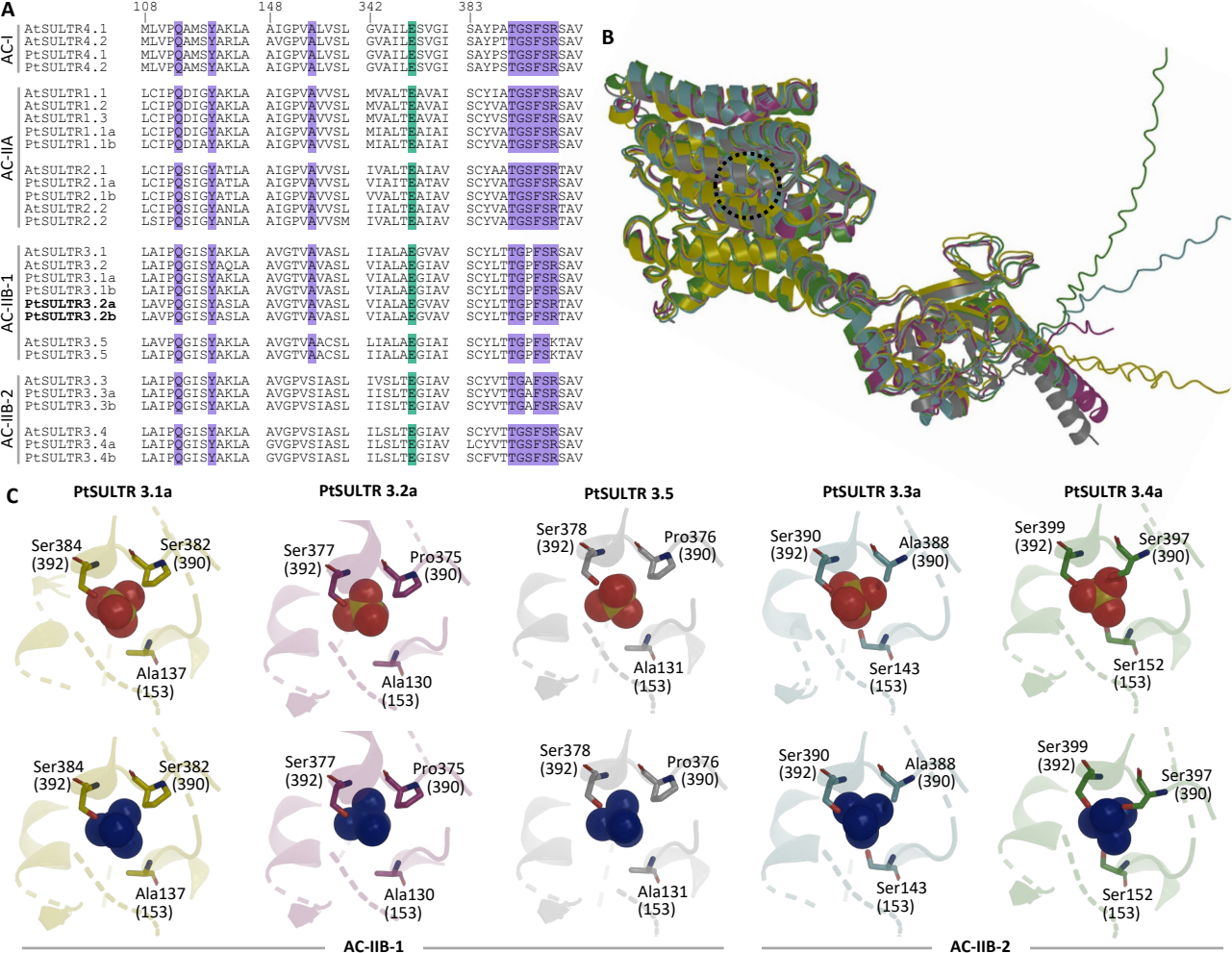
A
108
148
342
383
AC-I
AtSULTR4.1 MLVPQAMSYAKLA AIGPVALVSL GVAILESVGI SAYPATGSFSRSAV
AtSULTR4.2 MLVPQAMSYARLA AVGPVALVSL GVAILESVGI SAYPTTGSFSRSAV
PtSULTR4.1 MLVPQAMSYAKLA AIGPVALVSL GVAILESVGI SAYPSTGSFSRSAV
PtSULTR4.2 MLVPQAMSYAKLA AIGPVALVSL GVAILESVGI SAYPSTGSFSRSAV
AC-IIA
AtSULTR1.1 LCIPQDIGYAKLA AIGPVAVVSL MVALTEAVAI SCYIATGSFSRSAV
AtSULTR1.2 LCIPQDIGYAKLA AIGPVAVVSL MVALTEAVAI SCYVATGSFSRSAV
AtSULTR1.3 LCIPQDIGYAKLA AIGPVAVVSL MVALTEAVAI SCYVSTGSFSRSAV
PtSULTR1.1a LCIPQDIGYAKLA AIGPVAVVSL MIALTEAIAI SCYVATGSFSRSAV
PtSULTR1.1b LCIPQDIAYAKLA AIGPVAVVSL MIALTEAIAI SCYVATGSFSRSAV
AtSULTR2.1 LCIPQSIGYATLA AIGPVAVVSL IVALTEAIAV SCYAATGSFSRTAV
PtSULTR2.1a LCIPQSIGYATLA AIGPVAVVSL VIAITEATAV SCYVATGSFSRSAV
PtSULTR2.1b LCIPQSIGYATLA AIGPVAVVSL VVALTEAIAV SCYVATGSFSRSAV
AtSULTR2.2 LCIPQSIGYANLA AIGPVAVVSL IIALTEAIAV SCYVATGSFSRTAV
PtSULTR2.2 LSIPQSIGYANLA AIGPVAVVSM IVALTEAIAV SCYVATGSFSRTAV
AC-IIB-1
AtSULTR3.1 LAIPQGISYAKLA AVGTVAVASL IIALAEGVAV SCYLTTGPFSRSAV
AtSULTR3.2 LAIPQGISYAQLA AVGTVAVASL VIALAEGIAV SCYLTTGPFSRSAV
PtSULTR3.1a LAIPQGISYAKLA AVGTVAVASL VIALAEGIAV SCYLTTGPFSRSAV
PtSULTR3.1b LAIPQGISYAKLA AVGTVAVASL VIALAEGIAV SCYLTTGPFSRSAV
PtSULTR3.2a LAVPQGISYASLA AVGTVAVASL VIALAEGVAV SCYLTTGPFSRTAV
PtSULTR3.2b LAVPQGISYASLA AVGTVAVASL VIALAEGVAV SCYLTTGPFSRTAV
AtSULTR3.5 LAVPQGISYAKLA AVGTVAACSL LIALAEGIAI SCYLTTGPFSKTAV
PtSULTR3.5 LAIPQGISYAKLA AVGTVAACSL IIALAEGIAI SCYLTTGPFSKTAV
AC-IIB-2
AtSULTR3.3 LAIPQGISYAKLA AVGPVSIASL IVSLTEGIAV SCYVTTGAFSRSAV
PtSULTR3.3a LAIPQGISYAKLA AVGPVSIASL IISLTEGIAV SCYVTTGAFSRSAV
PtSULTR3.3b LAIPQGISYAKLA AVGPVSIASL IISLTEGIAV SCYVTTGAFSRSAV
AtSULTR3.4 LAIPQGISYAKLA AVGPVSIASL ILSLTEGIAV SCYVTTGSFSRSAV
PtSULTR3.4a LAIPQGISYAKLA GVGPVSIASL ILSLTEGIAV LCYVTTGSFSRSAV
PtSULTR3.4b LAIPQGISYAKLA GVGPVSIASL ILSLTEGISV SCFVTTGSFSRSAV
B
C
PtSULTR 3.1a
PtSULTR 3.2a
PtSULTR 3.5
PtSULTR 3.3a
PtSULTR 3.4a
Ser384 (392)
Ser382 (390)
Ala137 (153)
Ser377 (392)
Pro375 (390)
Ala130 (153)
Ser378 (392)
Pro376 (390)
Ala131 (153)
Ser390 (392)
Ala388 (390)
Ser143 (153)
Ser399 (392)
Ser397 (390)
Ser152 (153)
AC-IIB-1
AC-IIB-2

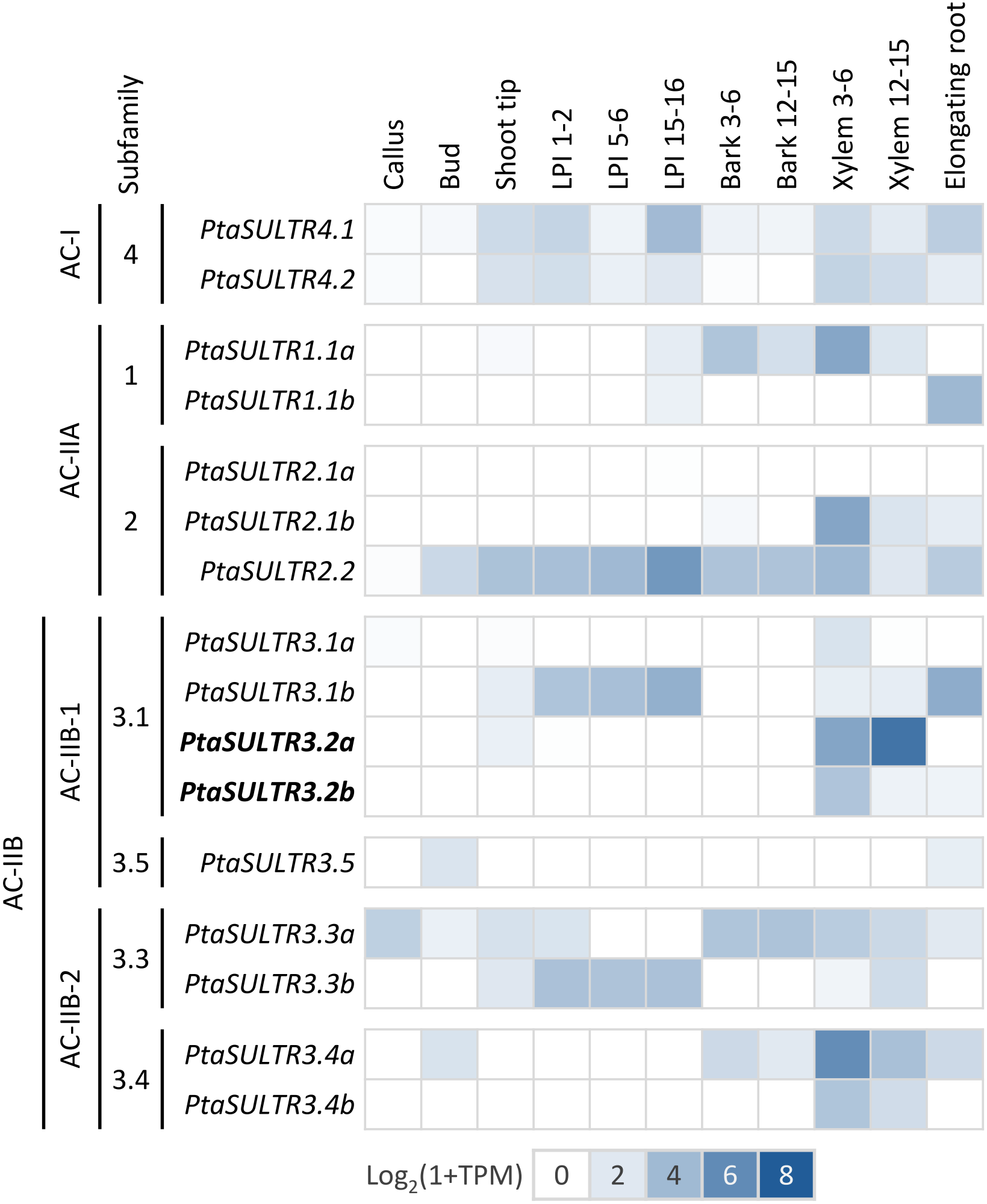
Subfamily
Callus
Bud
Shoot tip
LPI 1-2
LPI 5-6
LPI 15-16
Bark 3-6
Bark 12-15
Xylem 3-6
Xylem 12-15
Elongating root
AC-I
4
PtaSULTR4.1
PtaSULTR4.2
AC-IIA
1
PtaSULTR1.1a
PtaSULTR1.1b
2
PtaSULTR2.1a
PtaSULTR2.1b
PtaSULTR2.2
AC-IIB
AC-IIB-1
3.1
PtaSULTR3.1a
PtaSULTR3.1b
PtaSULTR3.2a
PtaSULTR3.2b
3.5
PtaSULTR3.5
AC-IIB-2
3.3
PtaSULTR3.3a
PtaSULTR3.3b
3.4
PtaSULTR3.4a
PtaSULTR3.4b
Log2(1+TPM)
0
2
4
6
8

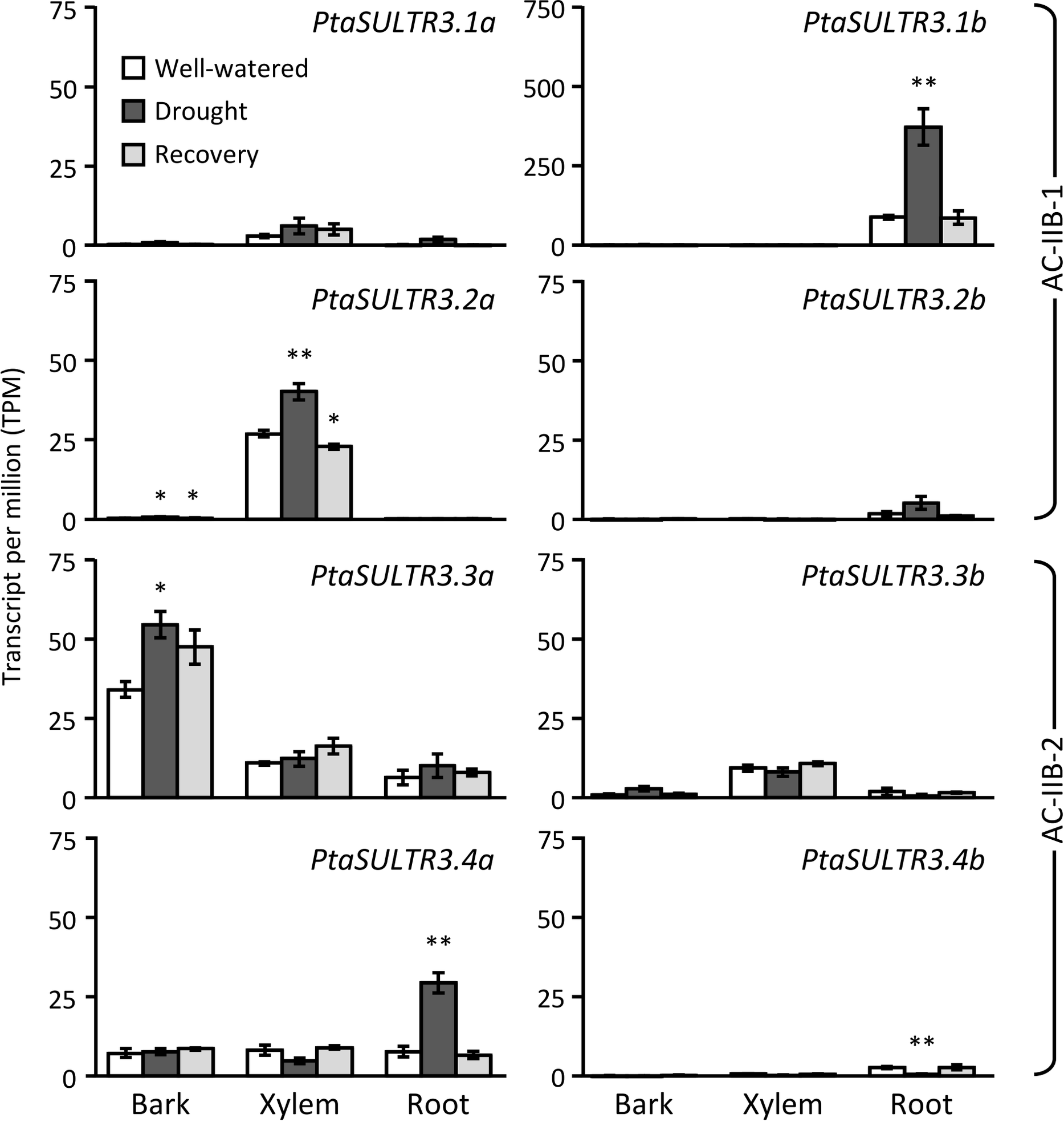
PtaSULTR3.1a
PtaSULTR3.1b
PtaSULTR3.2a
PtaSULTR3.2b
PtaSULTR3.3a
PtaSULTR3.3b
PtaSULTR3.4a
PtaSULTR3.4b
Well-watered
Drought
Recovery
Transcript per million (TPM)
AC-IIB-1
AC-IIB-2
Bark
Xylem
Root
0
25
50
75
250
500
750
*
**

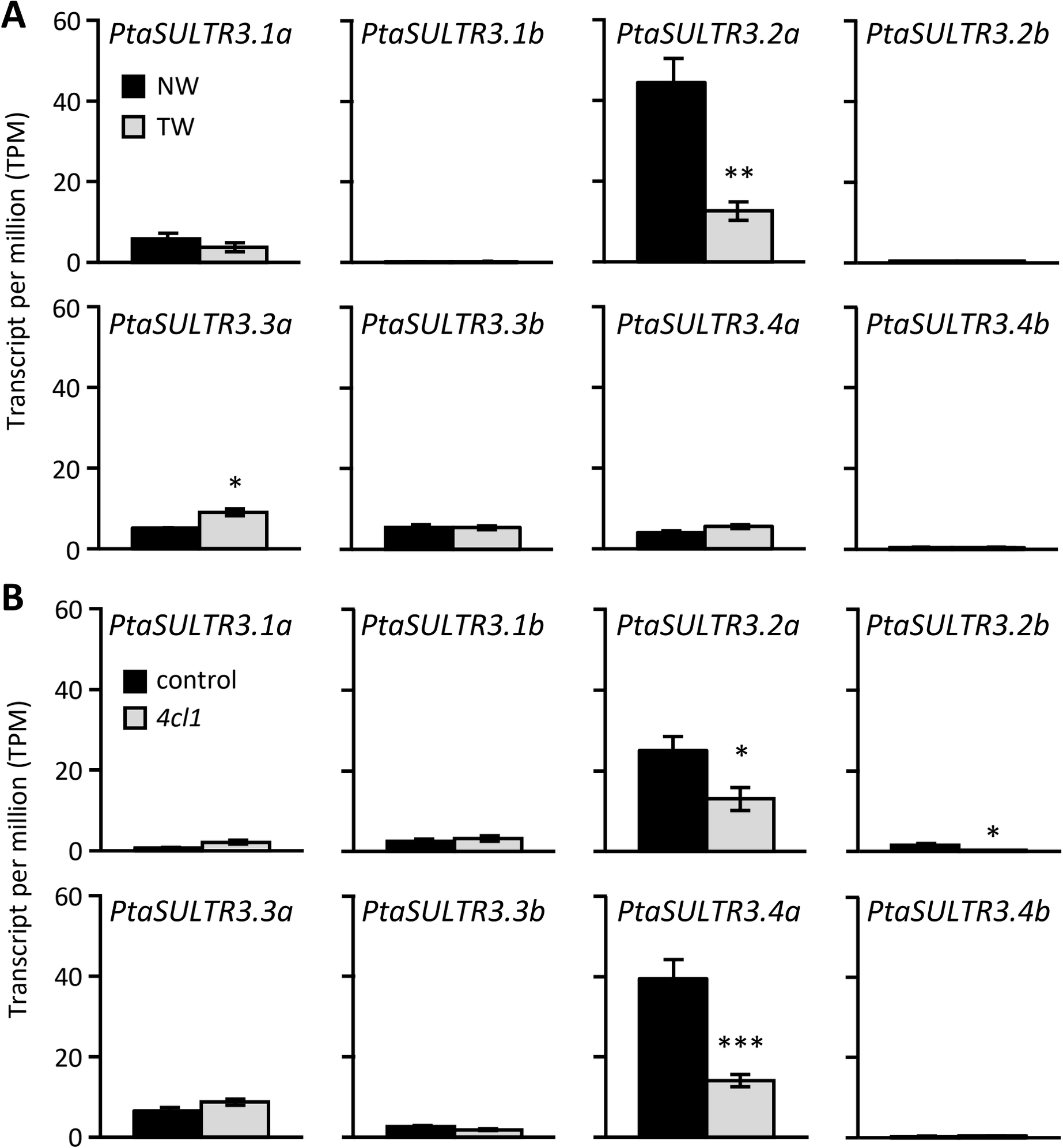
A
B
Transcript per million (TPM)
NW
TW
control
4cl1
PtaSULTR3.1a
PtaSULTR3.1b
PtaSULTR3.2a
PtaSULTR3.2b
PtaSULTR3.3a
PtaSULTR3.3b
PtaSULTR3.4a
PtaSULTR3.4b
0
20
40
60
*
**
***

C

		PAL2/4/5	C3H3	HCT1/6	4CL1/5	CCoAOMT1/2	CCR2	F5H1/2	COMT2	CAD1/2
	Δ lignin (%)	**-6.2**	**-7.9**	**-2.6**	**-5.8**	**-4.4**	*-2.1*	**-1.7**	**-4.3**	*-2.2*
Log_2 fold change	*SULTR3.2a*	*0.2*	**0.2**	-0.2	**-0.8**	*-0.8*	**-0.4**	0.1	**-0.5**	0.2
	SULTR3.4a	-0.1	**0.4**	0.1	**-1.7**	-0.8	**1.2**	**-0.5**	0.0	0.4

Table 1. SULTR family members in 22 plant species.

Species	AC-I	AC-IIA		AC-IIB				Total
				AC-IIB-1		AC-IIB-2		
	SULTR4	SULTR1	SULTR2	SULTR3.1	SULTR3.5	SULTR3.3	SULTR3.4	
Bryophyte								
Physcomitrium patens[a]	1	3[b]						4
Lycophyte								
Selaginella moellendorffii[a]	1	1[b]		2[c]				4
Angiosperms								
Amborella trichopoda[a]	1	1	1	1	1	1	1	7
Liriodendron tulipifera[a]	1	2	1	1	2	1	1	9
Eudicots								
Aquilegia coerulea[a]	1	1	0	2	1	1	1	7
Rosid								
Arabidopsis thaliana	2	3	2	2	1	1	1	12
Capsella rubella	2	3	2	2	1	1	1	12
Eucalyptus grandis	1	3	1	2	2	1	1	11
Glycine max	2	4	8	4	2	3	4	27
Medicago truncatula	1	3	4	2	1	2	2	15
Populus trichocarpa	2	2	3	4	1	2	2	17
Quercus rubra	1	4	2	2	1	1	1	12
Vitis vinifera	1	2	2	4	2	1	2	14
Asterids								
Lactuca sativa	2	4	2	1	3	1	2	15
Mimulus guttatus	1	6	2	3	1	1	2	16
Solanum lycopersicum	1	3	3	3	1	1	1	13
Monocots								
Ananas comosus[a]	2	2	1	1	1	1	1	9
Brachypodium distachyon	1	3	1	2	1	1	1	10
Oryza sativa	1	3	2	2	2	1	1	12
Pancicum virgatum	2	5	2	3	2	1	2	17
Sorghum bicolor	1	3	2	2	1	1	1	11
Zea mays	1	3	1	1	1	1	1	9
Total	29	64	42	46	28	24	29	262

[a] early-divergent species; [b] AC-IIA gene numbers in early-divergent species before the split of SULTR1 and SULR2; [c] AC-IIB gene number in *Selaginella moellendorffii* before the split of AC-IIB-1 and AC-IIB-2.